AD-A165 808 LASER METALWORKING TECHNOLOGY TRANSFER(U) AVCO EVERETT RESEARCH LAB INC EVERETT MA O A SANDVEN 1986 N00014-82-C-2373 1/1

UNCLASSIFIED F/G 11/6 NL

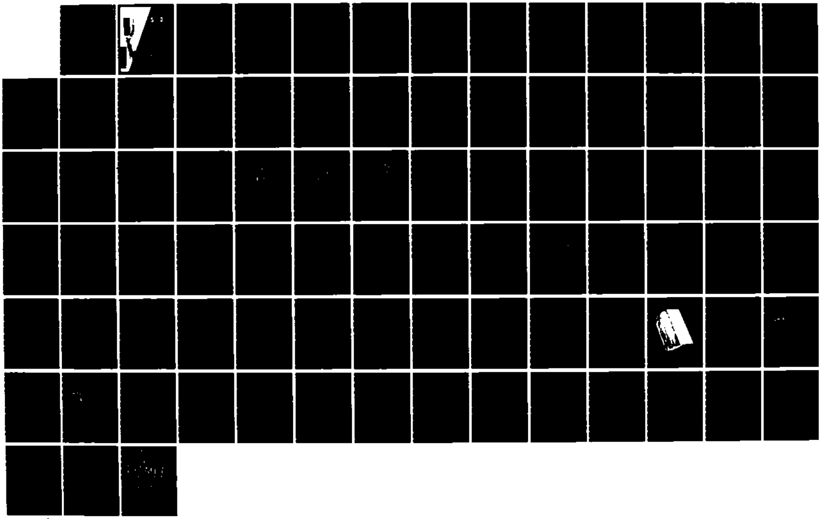

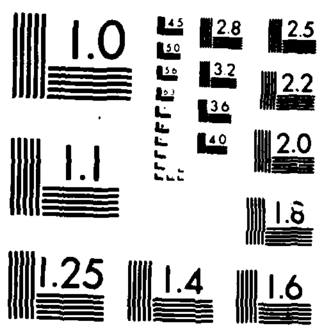

MICROCOPY RESOLUTION TEST CHART

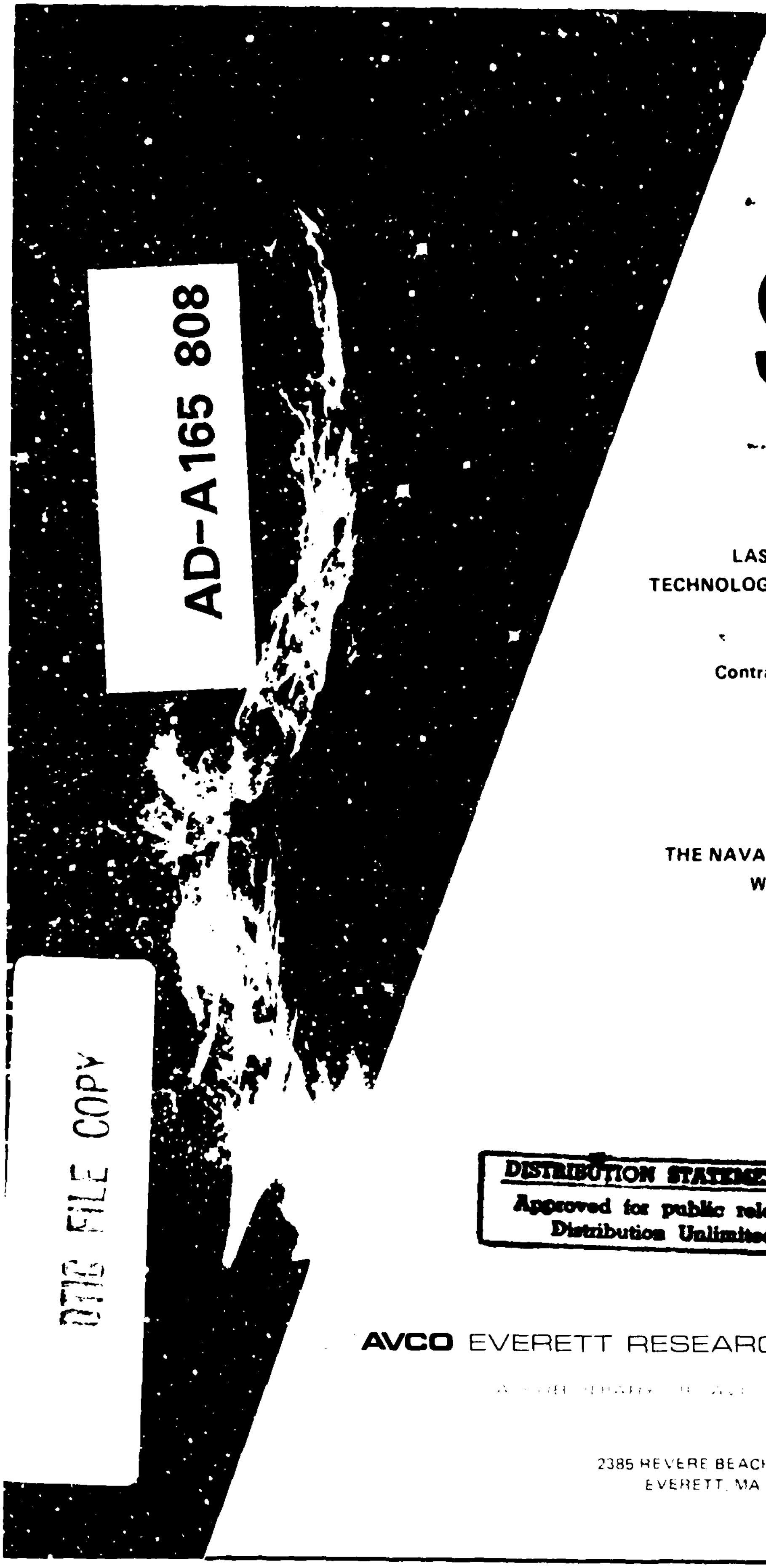

LASER METALWORKING TECHNOLOGY TRANSFER FINAL REPORT

Contract N00014-82-C-2373

prepared for

THE NAVAL RESEARCH LABORATORY
Washington, DC 20375

by

Ole A. Sanden

AVCO EVERETT RESEARCH LABORATORY, INC.

2385 REVERE BEACH PARKWAY
EVERETT, MA 02149

LASER METALWORKING TECHNOLOGY TRANSFER

FINAL REPORT

Contract N00014-82-C-2373

prepared for

THE NAVAL RESEARCH LABORATORY

Washington, DC 20375

by

Ole A. Sandven

Avco Everett Research Laboratory, Inc.

a Subsidiary of Avco Corporation

2385 Revere Beach Parkway

Everett, MA 02149

TABLE OF CONTENTS

TABLE OF CONTENTS
(cont.)

LIST OF ILLUSTRATIONS

LIST OF ILLUSTRATIONS
(cont.)

LIST OF TABLES

1. INTRODUCTION

The object of the Technology Transfer Program is to assist in the utilization and integration of the laser facility ~~at~~ FMC/NOD in~~to~~ the manufacturing process~~es~~ of naval ordnance components and systems.

This assistance consists of targeting workpieces and production steps suitable for laser processing in terms of cost effectiveness and quality enhancement, the development of techniques and procedures for such processing and the establishment of processing parameters and other pertinent data.

The work ~~performed~~ under this program has mainly ~~been~~ is related to laser surface transformation hardening of steels. The response of a number of frequently used steels to such laser processing has been determined over a wide range of processing parameters, models, and calculator programs for the prediction of laser hardening have been developed and tested, and the necessary thermophysical constants of the various materials determined by statistical and empirical means.

In addition to the transformation hardening survey, process development work relating to the laser hardfacing of aircraft carrier catapult rails have been performed, and preliminary techniques and processing data established for different combinations of hardfacing alloys/substrate materials.

All the laser processing performed in this program was carried out at Avco Everett Metalworking Laser facilities in Somerville, MA. An Avco HPL®-10 CO_2 laser with constant wave output was used throughout. Analysis of processing results was also done at AEML with the exception of some metallography and microhardness survey performed at FMC/NOD.

2. LASER SURFACE TRANSFORMATION HARDENING

2.1 General Considerations

2.1.1. The Process

Laser surface transformation hardening is a relatively new process, made possible by the development of high powered industrial lasers. As in other surface transformation hardening processes, the object of laser surface hardening is to generate a relatively thin surface layer in which the material has undergone martensitic transformation. The process is, therefore, limited to materials that are capable of undergoing such a transformation; or in other words, to hardenable cast irons and steels.

In order for such materials to harden by martensitic transformation, they must be heated to a temperature at which the austenitic phase is stable, followed by very rapid cooling, or quenching, to room temperature.

In surface hardening only the surface region of the workpiece needs to be heated to austenitizing temperatures. It is desirable that this surface heating takes place as rapidly as possible, in order to minimize the effect of heating on the bulk of the material. This requires a very high heat flux to be applied to the workpiece surface. In essence, heat must be applied to the surface at a higher rate than it can be conducted away from the surface towards the cold interior. This makes the laser an ideal heat source for surface hardening of cast irons and steels. In fact, the laser is capable of heating the surface so rapidly that the required subsequent quenching occurs by heat conduction to the still cold interior of the workpiece.

This process, known as self-quenching, is one of the great advantages of laser surface hardening.

When the laser is used for surface transformation hardening, the required power density (flux) is lower and the exposure time longer than in processes such as welding or cutting.

A convenient way of achieving this is to reshape the laser output beam to a broad area beam with uniform power density rather than to the focused beam used for welding and cutting. A typical broad area laser beam, suitable for surface transformation hardening, may have the shape of a square with dimensions of the order 1 cm x 1 cm in the focal plane, and have a power density of 5×10^2 to 5×10^3 w/cm^2. Hardening is performed by moving such a spot over the workpiece surface at controlled speed. If the processing parameters (power and speed) are appropriate, a strip of surface hardened material is generated by the moving laser spot, and the depth of this hardened case can be controlled through the control of these parameters.

The laser output beam can also be shaped into other suitable broad area beams by means of various optical devices, depending on the specific applications. However, in this program, a square spot with dimensions 1.27 cm x 1.27 cm (0.5" x 0.5") was used throughout.

The absorption of laser radiation from a CO_2 laser (10.6μm) in metals is very low at room temperature. With the relatively low power densities used in surface hardening, it is, therefore, necessary to use energy absorption coatings on the workpiece surface. Many different substances have been used for this purpose, such as manganese phosphate and paints containing graphite, silicon and carbon black. Since many of the coatings that have been used are quite effective, the choice of a particular coating is dictated not so much by its relative absorption efficiency, as by other considerations such as ease of application and post-processing removal of coating residue. In the work reported here, flat black Krylon #1602 spray paint was used. This coating appears to be 80-90% effective in overall absorption of the 10.6 μm laser radiation. It is easy to apply and is not very sensitive to variation in coating thickness, as long as care is taken to ensure complete coverage. The residue left by this coating after laser processing is also easy to remove.

2.1.2 Metallurgy

In conventional hardening of steel, the workpiece is brought up to austenitizing temperatures at a relatively slow rate, and then allowed to soak at this temperature before quenching. This allows sufficient time for homogenous austenite to form throughout the workpiece, which upon quenching will be transformed to martensite.

In laser surface transformation hardening, the situation is somewhat different because the heating time is very short and no isothermal soak takes place in this process. The very rapid heating and the short time that the workpiece material is kept at elevated temperatures result in several metallurgical effects which must be taken into consideration in analyzing the process.

First of all, rapid heating leads to an increase in the observed transformation temperature[1)], which can result in a thinner hardened case than otherwise would be expected. This effect will, of course, become more pronounced as the laser processing speed increases and the exposure time decreases.

Secondly, if the structure of the workpiece is such that the carbon is unevenly distributed in the micro-structure, the short time the material is at temperatures above the transformation temperature is not sufficient to allow the carbon to redistribute itself uniformly in the austenitic phase. The resulting austenite will, therefore, be of variable carbon content and the structure obtained after self-quenching will not be uniform[2]. This is not a problem with reasonably fine-grained, medium and high carbon steels, but if the material contains appreciable amounts of free ferrite, such as low carbon steel or some nodular cast irons, laser surface hardening may not be possible in practice. This is particularly so if the material is relatively coarse-grained. Such materials can, however, be laser hardened if they are given a pre-processing quench and temper heat treatment. If the tempering temperature is not too high such a material will have its carbon in a finely dispersed form, and can be laser surface hardened.

Because the laser hardening process takes place under conditions of unsteady heat flow, it is necessary to heat the workpiece surface to temperatures considerably above the normal austenitizing range, in order to obtain useful heat penetration and case depth. The surface will, therefore, experience much higher temperatures than in conventional hardening practices. Care must be taken to prevent the surface temperature from reaching the melting point, particularly in cases where a very deep case is to be generated.

In some cases, localized grain growth may occur if the surface temperature approaches the melting point. Because the maximum temperatures will often occur in the neighborhood of corners and fillets, such grain growth may be very detrimental.

There is also some indication that areas that have been brought to a very high temperature may show excessive amounts of retained austenite after quenching.

The depth of hardened case that can be obtained in laser surface transformation hardening also depends on the hardenability of the material and on the size of the workpiece. A large workpiece, made from a material with good hardenability, can be processed at low speed because a high rate of self-quenching is not required. Hence, there is sufficient time available for deep heat penetration and a deep case can be generated. In SAE 4340 steel, for example, case depths in excess of 0.1" are easy to obtain.

In materials with low hardenability, such as low carbon steel, the laser processing speed must be higher in order to obtain high self-quenching rates. This is particularly true if the workpiece is small and thus is a limited heatsink. A steep temperature gradient must be generated in the workpiece, but because the maximum surface temperature is limited by the melting point of the material, only limited hardened case can be obtained in such materials.

2.1.3 Heat Flow in Laser Surface Transformation Hardening

In order to predict the results of laser surface transformation hardening with a broad area beam, it is necessary to evaluate the time dependent temperature distribution in the workpiece in the vicinity of of the moving laser spot. Because the boundary conditions are favorable, it is possible to obtain closed solutions to the generalized heat flow equation

$$\alpha \nabla^2 T = \frac{\partial T}{\partial t} \qquad 1)$$

that are useful for such prediction. If we consider the semi-infinite body, Equation 1) reduces to

$$\frac{\partial Q}{\partial t} = \alpha \frac{\partial^2 Q}{\partial z^2} \qquad 2)$$

where α is the thermal diffusivity; Z, the depth below the surface; $Q = -K\ ^{\partial T}/_{\partial Z}$ is the flux and K is the thermal conductivity. If the flux at the surface is constant, the boundary conditions are:

The solution to Equation 2) is then[3]

$$\nabla T = \frac{2Q_i \epsilon}{K} \sqrt{\alpha t}\ ierfc\ \frac{z}{2\sqrt{\alpha t}} \qquad 3)$$

where ΔT at the temperature rise; Qi is the applied flux, ierfc stands for the integrated error function compliment and ξ is the emmisivity of the material, specific to temperature and wavelength of the laser radiation.

This solution is only valid for a semi-infinite body with uniform flux at the surface; i.e., when there is no lateral heat flow so that the heat flow is unidirectional.

This condition is, however, approximately true for the centerline of a broad area laser spot with uniform power distribution, provided the spot is large compared to the characteristic heat diffusion distance

$$d = (\alpha t)^{1/2} \qquad 4)$$

where t_D is the dwelltime (exposure time). For a square spot with dimensions bxb, this time is:

$$t_D = b/\nu \qquad 5)$$

where ν is the velocity of the laser spot. Hence, if

$$\frac{b}{2} \gg (\alpha t_D)^{1/2} \qquad 6)$$

Equation 3) will correctly give the temperature at the centerline of the laser spot. In practice, it is found that if $b \geq 16d/\nu$, good agreement with experimental data can be obtained. We can then rewrite Equation 3) in the form

$$T_T = T_0 + \frac{2Qi\varepsilon}{K}\sqrt{\alpha t_D}\; i\,\mathrm{erfc}\; \frac{S_H}{2\sqrt{\alpha t_D}} \qquad 7)$$

where T_T is the transformation temperature, T_o is the room temperature, and δH is the depth of case.

This equation can also be used to estimate the cooling rate resulting from the self-quenching effect behind the moving laser spot. By the superposition principle, the temperature on the centerline behind the laser spot is approximately:

$$T = T_0 + \frac{2Qi\varepsilon}{K}\left[\sqrt{\alpha t}\; i\mathrm{erfc}\,\frac{z}{2\sqrt{\alpha t}} - \sqrt{\alpha(t-t_D)}\; i\mathrm{erfc}\,\frac{z}{2\sqrt{\alpha(t-t_D)}}\right] \quad 8)$$

where t is the total elapsed time from the start of heating and $(t-t_D)$ is the cooling time. Because of the requirements for minimal lateral heat flow discussed above, this equation can only be used for high speed processing and small values of the cooling time $(t-t_D)$.

If the processing speed is so low that Equation 7) cannot be used; that is, if the heat flow is three-dimensional in the vicinity of the centerline of the laser spot, a more involved analysis is required. An expression, valid for the semi-infinite body with three-dimensional flow around a rectangular spot, is given by Carslaw and Jaeger [4]. A modification, derived on slightly different principles and valid for a plate with finite thickness was developed in conjunction with this program. The temperature distribution around the moving laser spot under these conditions, was found to be [5]

$$T = T_0 + \frac{Qi\varepsilon\alpha}{2Kv\sqrt{\pi}} \int_0^1 \sum_{m=-\infty}^{m=\infty} \exp -\left[\frac{(2mD-z)\omega}{1-\omega}\right]^2 \cdot \left[\mathrm{erf}\,\frac{(Y+L)\omega}{1-\omega} - \mathrm{erf}\,\frac{(Y-L)\omega}{1-\omega}\right] \cdot \left[\mathrm{erf}\,\frac{2(X+B)\omega^2-(1-\omega)^2}{2\omega(1-\omega)} - \mathrm{erf}\,\frac{2(X-B)\omega^2-(1-\omega)^2}{2\omega(1-\omega)}\right]\frac{d\omega}{\omega^2} \quad 9)$$

where erf stands for the error function and:

$$X = \frac{\nu x}{2\alpha} \qquad B = \frac{\nu b}{4\alpha}$$

$$Y = \frac{\nu y}{2\alpha} \qquad L = \frac{\nu \ell}{4\alpha}$$

$$Z = \frac{\nu z}{2\alpha} \qquad D = \frac{\nu d}{2\alpha}$$

b = length of laser spot.
ℓ = width of laser spot.
d = thickness of plate.

In using these models for the prediction of hardened case, it is necessary to know the intensity of the actually absorbed flux, the average value of the thermophysical constants K and α (thermal conductivity and thermal diffusivity) in the temperature range experienced by the workpiece during processing, and the temperature at which the material will transform to austenite.

The fraction of the applied power that is absorbed into the workpiece (the emissivity ξ), depends among other things on the condition of the workpiece surface. For clean metal surfaces, the emissivity at the wavelength of the CO_2-laser (10.6 μm) is very low. However, by using various absorbing coatings, the emissivity can be increased to the 0.8-0.9 range, even at the relatively low power densities used in surface hardening. In this work, flat black Krylon #1602 spray paint was used as an energy absorber. This increased the absorption to an estimated value of 85%.

The values of the thermal conductivity, K, and the thermal diffusivity, α, for hardenable ferrous materials, changes fairly rapidly with the temperature. Hence, the room temperature values of these variables cannot be used for case depth prediction.

However, in cases where the variation of K and α with the temperature are known, the integral average value can be calculated as:

$$\overline{K} = \frac{1}{T_2 - T_1} \int_{T_1}^{T_2} V(T)\, dT \qquad 10)$$

$$\overline{\alpha} = \frac{1}{T_2 - T_1} \int_{T_1}^{T_2} \alpha(T)\, dT \qquad 11)$$

by means of numerical integration.

In this work, case prediction was performed partially by the aid of Equation 9) and 10), partially by experimental determination of K and α from preliminary runs, as described in Section 2.2.5.

The final datum needed for case prediction is the transformation temperature. This is, of course, not a fixed temperature unless the steel has eutectoid composition. Furthermore, the temperature range over which the transformation occurs is sensitive to the processing speed. In this work, we have used the A_f temperatures from the pertinent IT diagrams as the transition temperature T_T.

2.2 Experimental Work

2.2.1 Equipment and Procedures

The experimental surface transformation hardening was performed with an Avco HPL®-10 CO_2 laser. This laser was capable of up to 15 kW output (CW).

The collimated output beam from the laser was directed through ducts to the workstation. In the workstation, the beam - approximately 2.6" in diameter - was shaped to a convergent, square beam by means of an optical integrator, as shown in Figure 1. The square beam had dimensions 1/2" x 1/2" in the focal plane.

Surface transformation hardening was performed on plane specimens by moving the specimens under the beam at controlled speed. The specimens were mounted on a milling machine table in such a way that the focal plane of the optical integrator was located on the specimen surface. The translation speed of the table could be varied steplessly, and speed calibration curves were established prior to start of processing. The correct location of the specimen relative to the beam could be determined by means of a low powered He-Ne laser locator beam built into the laser system to give a visual representation of the location of the actual power beam prior to processing.

The laser power could also be varied steplessly, from approximately 1 kW up to full power. The actual power delivered to the workpiece was determined by calibration curves, established in advance by means of calorimetric measurements. In addition, the beam quality (sharp edges and even power density) was assessed by making test burns in lucite blocks. Speed and power calibration, as well as beam quality, was checked periodically during processing of the samples. Figure 2 shows schema-

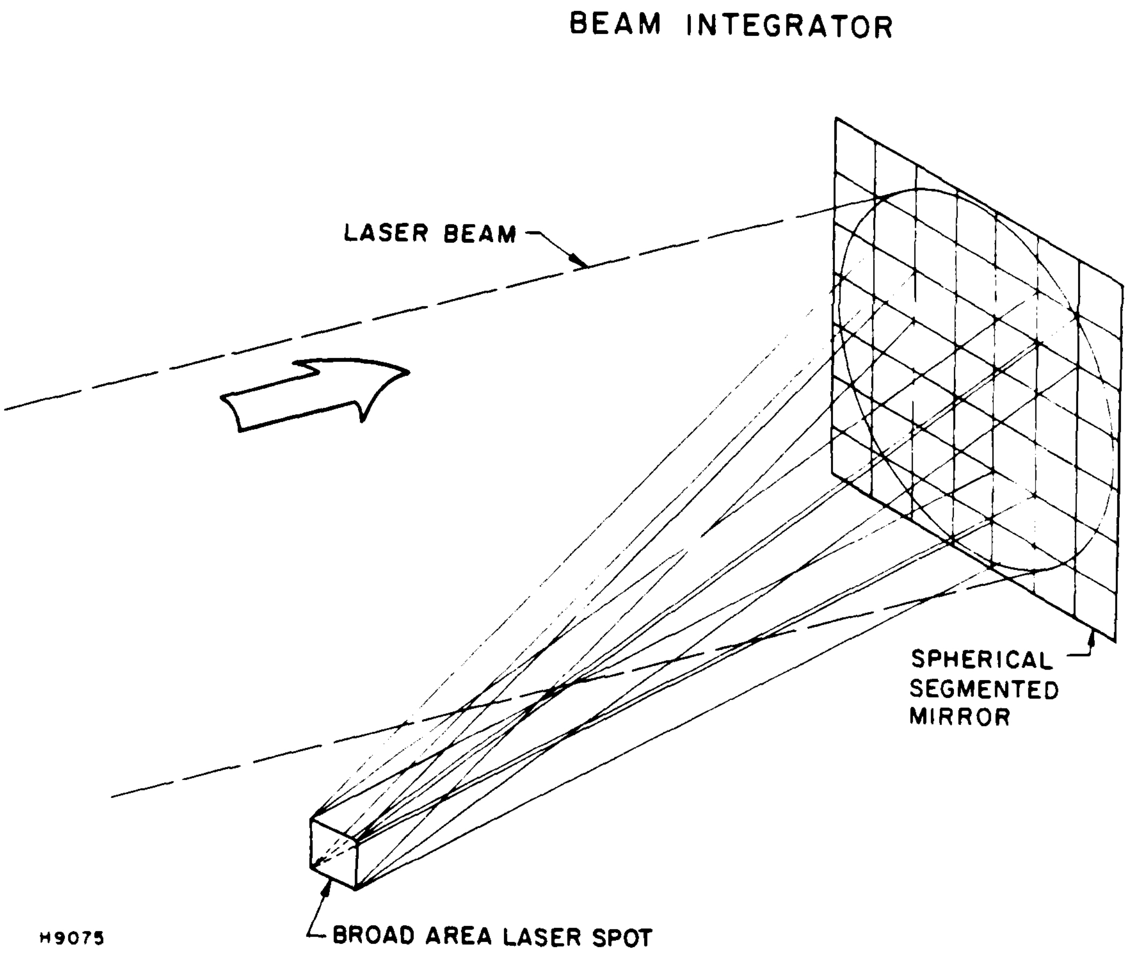

FIGURE 1 FORMING A BROAD AREA LASER SPOT BY MEANS OF AN OPTICAL INTEGRATOR

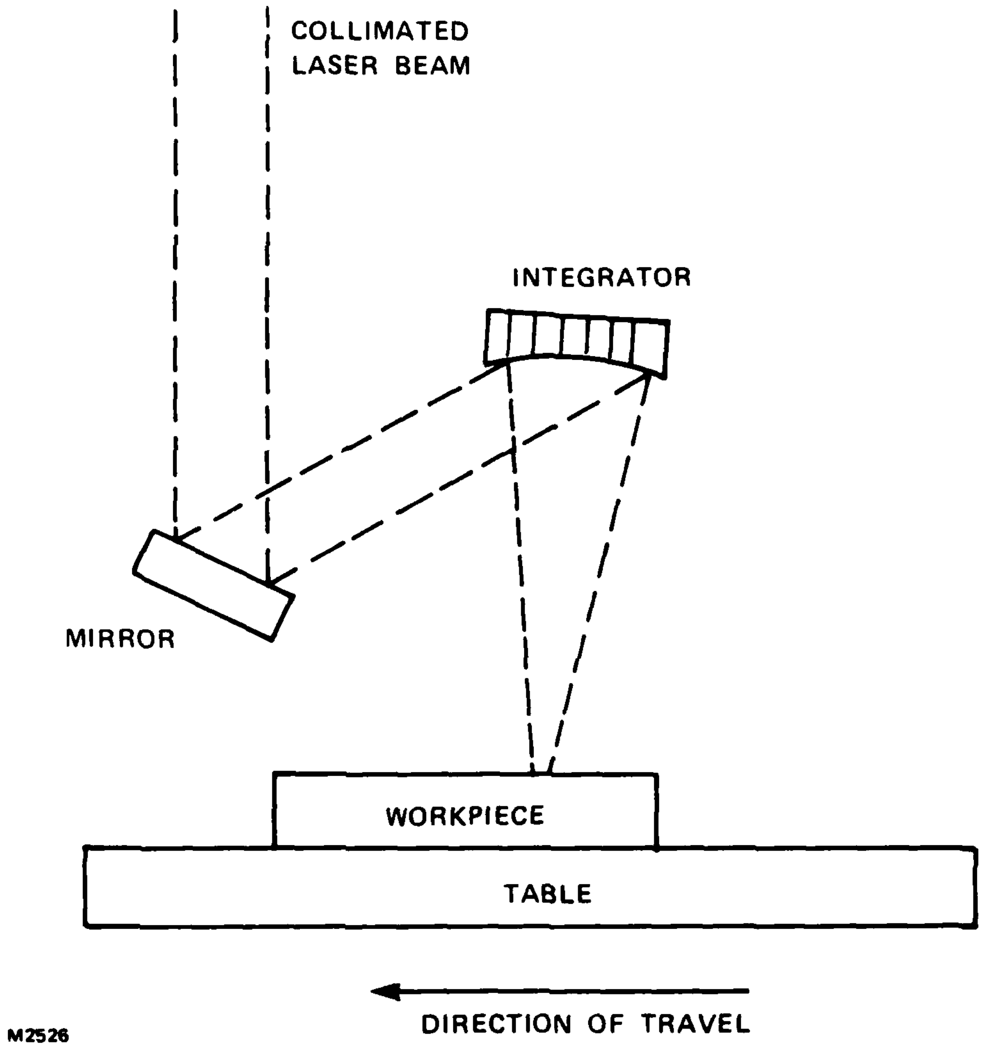

FIGURE 2 SETUP FOR LASER TRANSFORMATION HARDENING OF FLAT PLATES

tically the experimental setup used for this program.

Prior to processing, the workpiece surfaces were prepared by coating with flat black Krylon #1602 spray paint. This was done in order to enhance the absorption of the laser radiation (10.6 μm) into the workpiece surface. Previous experience has shown that this treatment results in approximately 85% absorption of the CO_2 laser radiation, even at relatively low power densities. Furthermore, this type of coating is easy to put on, leaves little residue for post-processing cleanup, and is not very sensitive to small variation in application technique. No protective atmosphere was used during processing, but a fan blowing crosswise over the beam/workpiece interaction zone was used to dissipate the smoke resulting from pypolysis of the coating.

The results of the laser processing were evaluated by metallography and micro-hardness testing, using a Knoop Indenter with 500g load.

2.2.2. Case Prediction by One-Dimensional Heat Flow Model

Prior to the experimental laser processing, the processing parameters were estimated, using a calculator code built on one-dimensional heat flow considerations, as discussed in Section 2.1.2.

The program was written for use on a Texas Instrument TI 59 programmable calculator/printer. This program predicted maximum surface temperature and depth of case based on processing parameters (speed and power density), thermophysical constants and transition temperature of the material.

Originally, this program did not contain any cutoff for processing parameters that fell outside the range where the one-dimensional heat flow model was valid. The predicted case depth did not, therefore, show reasonable agreement with experimentally obtained data for low processing speed. The program was, subsequently, rewritten to reject input data of this kind. The program could also be used to predict cooling rates during self-quench, based on Equation 8), Section 2.1.3.

The flow sheet of the program is shown in Figure 3, and the complete program with user information is listed in Appendix I.

The thermophysical constants used in the preliminary phase were calculated from published data [6)], as described in Section 2.1.3. The constants for the materials surveyed in the preliminary phase are given in Table I.

2.2.3. Preliminary Evaluation of Laser Hardening Parameters

In this preliminary evaluation phase, the response of six different materials to laser surface hardening was surveyed. The materials were SAE 1045 in the quenched and tempered condition (Q/T), SAE 1045 in the hot-rolled condition (H.R.), SAE 4140 in the Q/T and H.R. condition, SAE 1020 in the H.R. condition and SAE 4340 in the cold-rolled condition (C.R.). Samples of these materials were supplied by FMC/NOD in the form of plates with minimum dimensions 1/2" thick by 2" wide by 8" long.

These specimens were laser processed as described earlier, making single, well separated straight laser runs on the surfaces of the specimens. The processing parameters (power and speed) were varied within limits, calculated to give case depths in the range 10 to 120 mil (0.025 to 0.305 cm). The predicted case was calculated in advance in each case, using the calculator program described in Section 2.2.2.

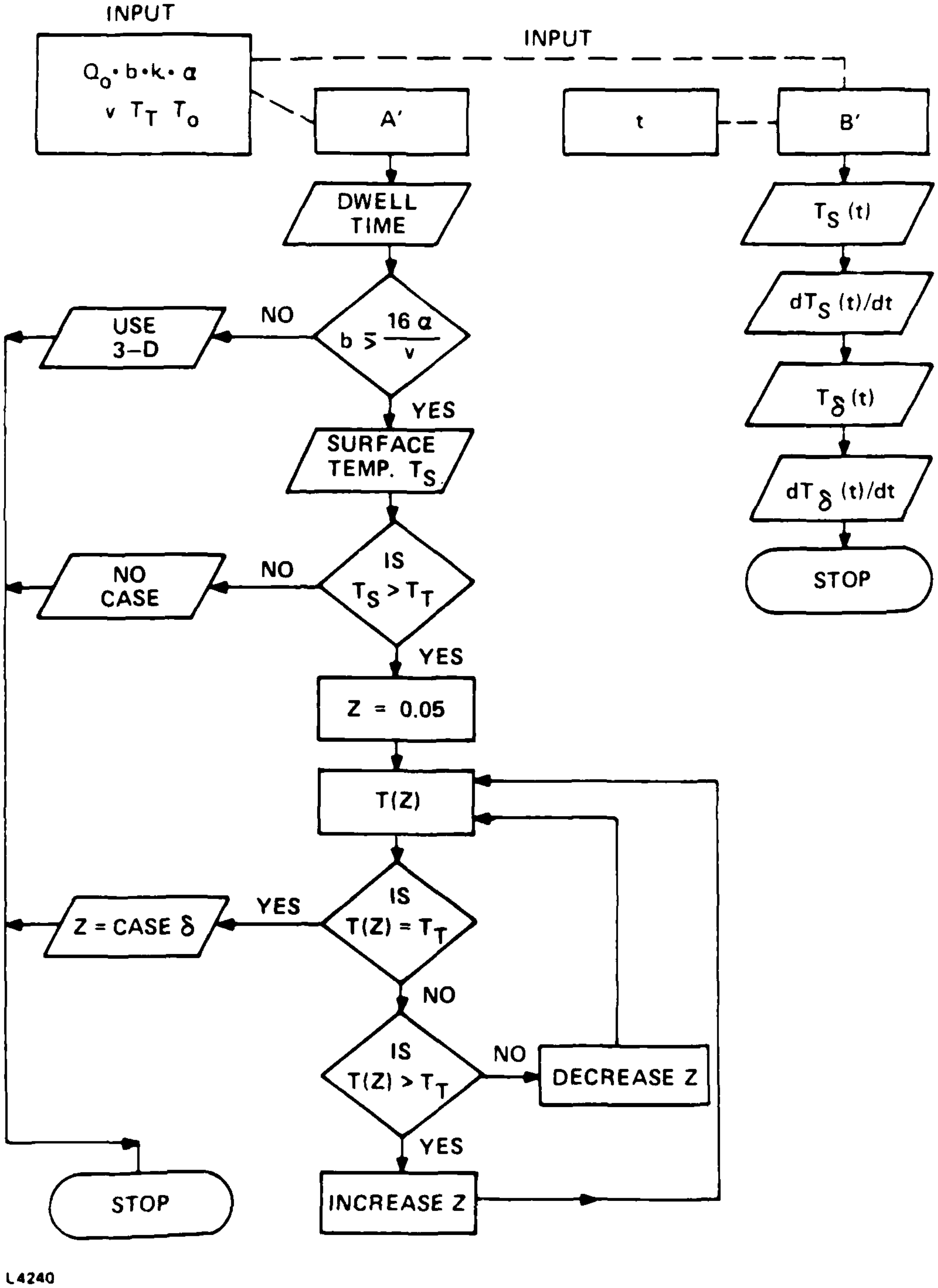

FIGURE 3 PROGRAM FOR PREDICTION OF CASE DEPTH AND COOLING RATE

TABLE I

THERMOPHYSICAL CONSTANTS (Estimated) FOR VARIOUS STEELS

Material	Thermal Cond. K (w/cm-C°)	Thermal Diff. α (cm^2/sec)	Transition Temp. T_T C°
SAE 1020	0.38	0.087	850
SAE 1045	0.36	0.085	790
SAE 4140	0.33	0.072	780
SAE 4340	0.30	0.063	750

The processed specimens were analyzed at FMC/NOD for case depth and surface hardness. The results are given in a preliminary report[7] from FMC/NOD, and are summarized in Tables II, III, IV and V. Due to the limits set by the total available laser power, large areas cannot be laser hardened without some form of multiple-pass technique. It is, however, of interest to look at the best way of achieving this. Several straight abutting and overlapping laser runs were made on samples of SAE 4140 (Q/T), and the discontinuity of hardened case in the zones between the runs assessed by surface hardness measurements. The results are shown in Figures 4, 5 and 6.

2.2.4 Discussion of Preliminary Results

The results of the preliminary processing, as given in Tables II through V, show good agreement between predicted and measured case for medium processing speed. The correlation is, however, poor for very high speed (60 in/min, 2.54 cm/sec) and for very low speed (5-10 in/min, 0.21-0.42 cm/sec). For the high speed runs the casedepth is much higher than predicted; while for low speed, the reverse is the case. The latter observation can be attributed to the fact that the one-dimensional heat flow model used is not valid at these low speeds. Hence, the actual temperatures reached by the workpiece surface are much less than those predicted, due to lateral heat flow in the workpiece.

The underestimation of case depth for the high speed runs is unexpected and difficult to explain. If anything, a shallower depth than predicted would not be surprising in this case because the heating rate is so rapid that the kinetics of the process could be expected to influence the results. Lacking any rational explanation for this phenomenon, it is, therefore, assumed that some

115% OF THEORETICAL
STANDARD DEVIATION
59.6%

SAE 4140

$\alpha = 0.072\ cm^2/sec$
$T_T = 780°\ C$

CONDITION	POWER (kW)	SPEED (in/min)	CALCULATED CASE (mil)	MEASURED CASE (mil)	% OF THEORETICAL	CALCULATED SURFACE TEMP. (C°)	SURFACE HARDNESS (Rc)
Q/T	2.5	30	49	47	96	1203	57
Q/T	2.5	40	29	37	128	1045	56.5
Q/T	2.5	60	8	18	225	856	57.5
Q/T	2.0	15	88	77	88	1369	55.5
Q/T	1.7	15	66	63	95	1174	56.5
Q/T	1.5	15	48	45	94	1045	55.5
Q/T	1.4	10	95	56	59	1275	56.5
H.R.	2.5	30	49	48	98	1203	43.5
H.R.	2.5	40	29	40	138	1045	45.0
H.R.	2.5	60	8	22	275	856	27.0
H.R.	2.0	15	88	71	81	1369	37.0
H.R.	1.7	15	66	54	82	1174	31.5
H.R.	1.5	15	48	45	94	1045	31.5
H.R.	1.4	10	95	53	57	1275	37.5

SAE 1045

$\alpha = 0.085\ cm^2/sec$

$T_T = 790°\ C$

144% OF THEORETICAL
STANDARD DEVIATION
90.1%

CONDITION	POWER (kW)	SPEED (in/min)	CALCULATED CASE (mil)	MEASURED CASE (mil)	% OF THEORETICAL	CALCULATED SURFACE TEMP. (C°)	SURFACE HARDNESS (Rc)
Q/T	2.5	30	51	50	98	1198	55
Q/T	2.5	40	30	38	127	1040	57
Q/T	2.5	60	7	24	342	853	55.5
Q/T	2.5	28	57	67	118	1239	55.5
Q/T	2.3	60	NIL	16	-	769	55.5
Q/T	2.1	40	13	20	154	882	55.5
Q/T	3.0	40	51	51	100	1278	54
H.R.	2.5	30	51	46	90	1198	47.5
H.R.	2.5	40	30	34	113	1040	50
H.R.	2.5	60	7	24	342	853	44
H.R.	3.0	40	51	51	100	1278	50

SAE 1020

83% OF THEORETICAL
STANDARD DEVIATION
8.3%

α = 0.087 cm^2/sec
T_T = 850° C

CONDITION	POWER (kW)	SPEED (in/min)	CALCULATED CASE (mil)	MEASURED CASE (mil)	% OF THEORETICAL	CALCULATED SURFACE TEMP. (C°)	SURFACE HARDNESS (Rc)
C.R.	1.9	30	6	NIL	-	887	31
C.R.	2.1	30	18	17	94	975	40
C.R.	2.3	30	29	25	86	1062	43
C.R.	2.45	30	38	27	71	1150	46
C.R.	2.6	30	47	38	81	1273	46.5

SAE 4340

86.7% OF THEORETICAL
STANDARD DEVIATION
24.3%

$\alpha = 0.063\ cm^2/sec$
$T_T = 750°\ C$

CONDITION	POWER (kW)	SPEED (in/min)	CALCULATED CASE (mil)	MEASURED CASE (mil)	% OF THEORETICAL	CALCULATED SURFACE TEMP. (C°)	SURFACE HARDNESS (Rc)
C.R.	2.4	30	49	45	92	1190	49.5
C.R.	2.3	40	27	26	96	992	51
C.R.	2.3	60	7	10	143	814	48.5
C.R.	1.6	10	110	75	68	1393	53
C.R.	1.6	15	63	54	86	1141	53
C.R.	1.4	15	45	40	89	1007	48.5
C.R.	1.9	15	85	73	86	1341	55
C.R.	1.3	10	78	55	71	1148	48
C.R.	1.0	5	116	57	49	1175	52.5

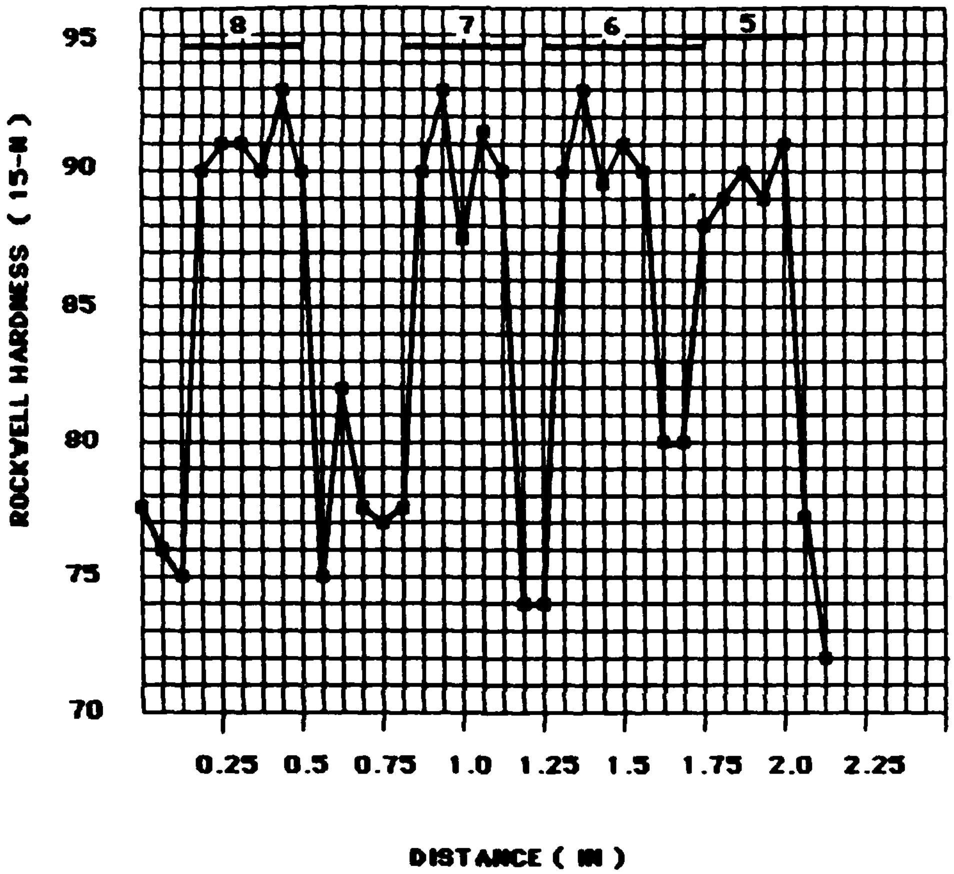

FIGURE 4.

SURFACE HARDNESS OF OVERLAPPING RUNS ON
SAE 4140 STEEL (H.T.)
POWER DENSITY 1290 W/cm ^{2}
PROCESSING SPEED 40 IN/MIN
RUNS 5-8

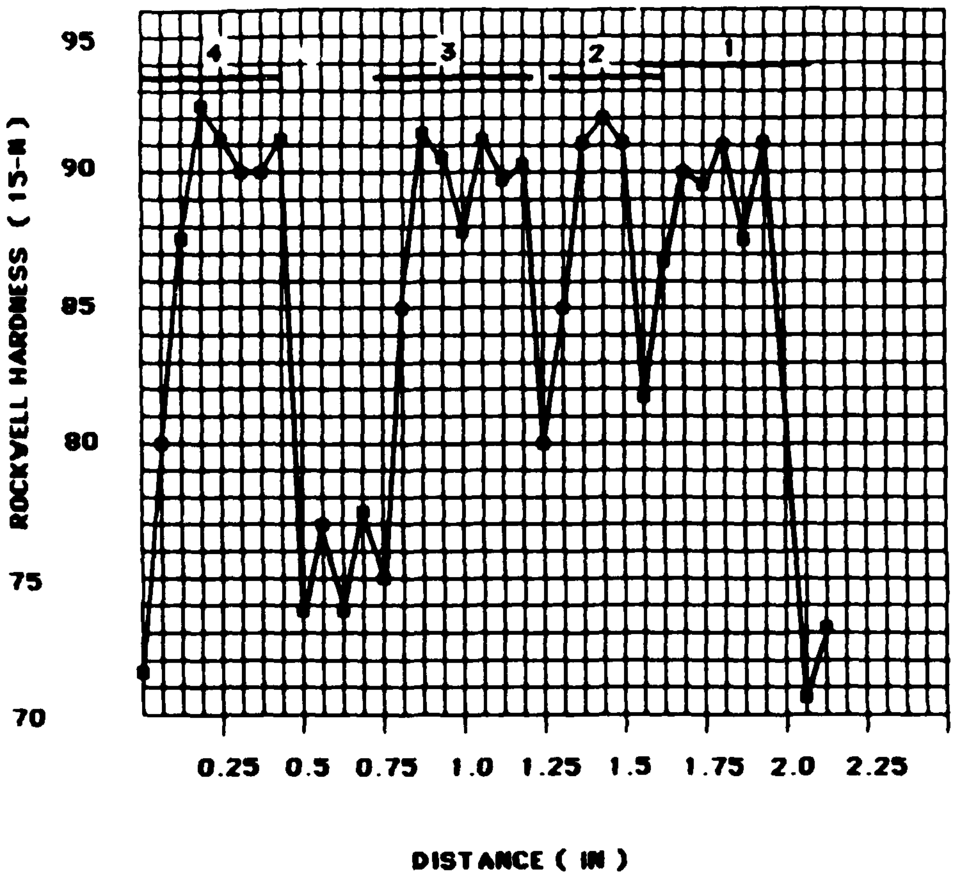

FIGURE 5

SURFACE HARDNESS OF OVERLAPPING RUNS ON SAE 4140 STEEL.
POWER DENSITY 1290 w/cm^2
PROCESSING SPEED 30 IN/MIN.
RUNS 1-4.

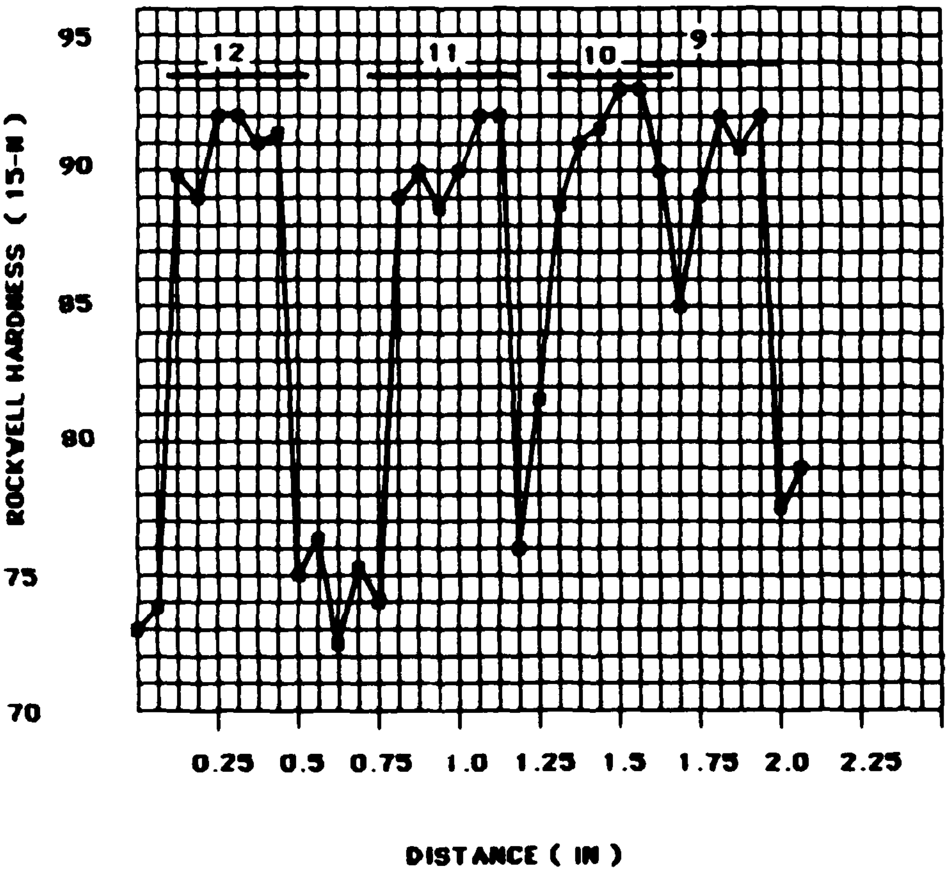

FIGURE 6.

SURFACE HARDNESS OF OVERLAPPING RUNS ON
SAE 4140 STEEL.(H.T.)
POWER DENSITY 790 W/cm^2
PROCESSING SPEED 15 IN/MIN.
RUNS 9-12

error was made in the power setting, or more possible in the speed calibration curve, in such a way that the actual translation speed was lower than the assumed speed.

For most of the materials, the limit of effective case was taken to be the depth at which the hardness had decreased to Rockwell C 45. In SAE 1020, this criterion could not be used, since the maximal hardness at 100% martensite is about equal to this. Hence, in this case, Rockwell C 35 was used as limit of effective case.

Several of the materials, in particular SAE 4140 (H.R.) and SAE 1045 (H.R.), showed very low surface hardness. This was due to some surface decarburization in these materials. Both materials showed full hardness at greater depth below the surface.

These preliminary studies show the need for the following improvements in the procedures used for the materials response survey:

- elimination of decarburized surface layers in the test specimens,
- improved model for case prediction, including better data for the thermophysical constants,
- closer control of processing parameters, particularly processing speed.

The results of the overlap runs, given in Figures 4,5 and 6, show that uniform hardened case across the specimen surface cannot be obtained with parallel, multiple laser runs. If the runs are overlapping, some backtempering will occur in the overlap zone. The minimum hardness in this zone is, however, well above the bulk hardness. Hence from the criterion of surface hardness alone, overlapping runs appear to be more effective than abutting or adjacent runs.

2.2.5 Improved Model for Prediction of Case Depth

As explained in Section 2.1.2., it is possible to obtain a closed solution to the heat flow equation, even if the conditions for one-dimensional heat flow are not met. The solution to the three-dimensional heat flow around a rectangular laser spot on the surface of a finite plate, Equation 9), is, however, very complex and time-consuming to use for practical purposes. It can be simplified somewhat by assuming the workpiece to be infinitely thick. (This is a valid assumption for the range of processing parameters used in this work, provided the actual plate thickness is not less than 1/4"). Furthermore, since a square spot is used in this work and we can limit our calculations to points on or below the centerline of the laser spot, we can rewrite Equation 9) in the form:

$$T = T_0 + \frac{2Qi\epsilon\alpha}{2K_1 v\sqrt{\pi}} \int_0^1 \exp - \left[\frac{z a}{1-a}\right]^2 \cdot \left[\operatorname{erf}\frac{L a}{1-a}\right] \cdot \left[\operatorname{erf}\frac{2(x+B)a^2+(1-a)^2}{2a(1-a)} - \operatorname{erf}\frac{2(x+B)a^2+(1-a)^2}{2a(1-a)}\right]\frac{da}{a^2} \qquad 12)$$

This is still a formidable expression to evaluate because the numerical integration requires some 50 to 100 ordinate evaluations in order to give sufficient accuracy. Furthermore, we are interested in finding the maximum value of the temperature relative to the laser spot, and we have no a priori knowledge where this maximum occurs. To make the model more readily useful, the following procedure was adopted. First, the temperature maximum on or directly below the centerline was evaluated for various paired values of the parameters B and Z in the speed region where three-dimensional heat flow dominates.

Secondly, by comparing these results to those obtained through the use of the one-dimensional heat flow equation (Equation 2), it was found that the ratio f between these two values

$$f = \frac{T(3-D)}{T(1-D)} \qquad 13)$$

could be expressed with good accuracy as a polynomial in the form:

$$f = \left(a_1 B^2 + b_1 B + C_1\right)\left(Z/B\right)^2 + \left(a_2 B^2 + b_2 B + C_2\right)\cdot\left(Z/B\right) + \left(a_3 B^{-2} + b_3 B^{-1} + C_3\right) \qquad 14)$$

provided the range of B values in each case was not too large. By dividing the range of B values between 0.5 and 4 into three intervals, the constants in Equation 14) could be found by regression analysis.

For values of $B \geq 4$, f is unity; i.e., the one-dimensional heat flow model is valid. A calculator program, incorporating Equation 14), could then be written in such a way that case depth values could be predicted for the entire range of processing parameters used in this work. The flow sheet of the program is shown in Figure 7, and the complete program with used instructions is listed in Appendix II.

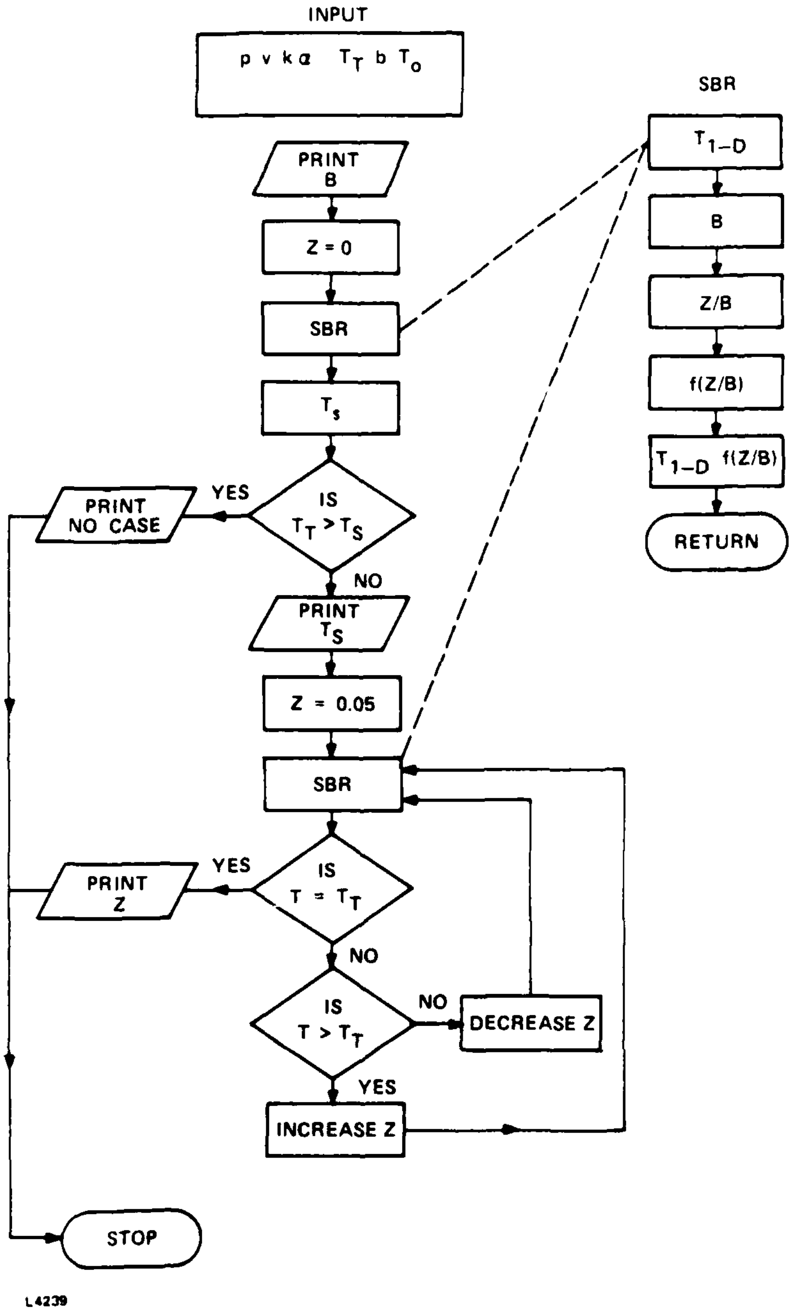

FIGURE 7 IMPROVED PROGRAM FOR CASE DEPTH PREDICTION

2.2.6. Experimental Evaluation of the Thermophysical Constants

As discussed in Section 2.1.2., the thermophysical constants K and α can be estimated for the purpose of case depth prediction, by calculating the integral average of these constants over the approximate temperature range of processing. Unfortunately, however, adequate data for the variation of K and α with the temperature is only available for a few steels. This is particularly true for the diffusivity α. To obtain more general and realistic values for K and α, the following procedure was adopted for the final phase of this work.

1) The thermal conductivity K was determined as before by calculating the integral average over the temperature range of processing, using published data and Equation 10). For materials where only the room temperature conductivity was available, the average value of K was estimated from this datum, relative to materials for which complete data was known.

2) A number of trial laser runs were made, using processing speeds sufficiently high to ensure predominantly one-dimensional heat flow. The resulting case depths were measured by means of micro-hardness testing, and the value of the diffusivity α for each material was then found by least mean square analysis, using the experimentally determined case depths and the value of conductivity K, (found from step 1) in Equation 7). Due to the transcendental nature of this equation, the analysis had to be done by numerical methods. This method of determining the average thermal

diffusivity is phenomenological and is not intended to represent anything else but an empirical parameter for practical work. The method has the advantage of expressing the value of α based on actual processing, and an error in the estimation of K will, at least in part, be compensated for due to the fact that the results obtained through Equation 7) are more dependent on the ratio of K and α then on their individual values. The values of K and α used in the final part of this work are given in Table VI. Some of the values for K, given in Table I, have been recalculated over a larger temperature interval and are, therefore, somewhat smaller. Here, it is noticeable that the new values of α, found by experimental methods, are significantly lower than the earlier values found by integral averaging.

2.2.7. Final Evaluation of Processing Parameters

In this final phase, steels in various heat treated conditions were laser processed over a wide range of processing parameters. The sample materials consisted of SAE 1045 in the annealed (ANN.) condition, the quenched and tempered (Q/T) condition and in the hot-rolled (H.R.) condition, SAE 4140 in the ANN., Q/T and H.R. condition, SAE 4340 in the ANN., Q/T and H.R. condition, SAE 8620 in the ANN. and Q/T condition, and Hyten B 3X in the ANN. and Q/T condition. Samples of SAE 1020 and SAE 4130 were also supplied by FMC/NOD, but these materials were not suited for parameter development work, as explained in Section 2.2.8 below. The samples consisted of plates and bars, none with thickness less than 1/2". All samples were processed in the same manner described in Section 2.2.1. In each case, the expected case depth was

TABLE VI

THERMOPHYSICAL CONSTANTS

MATERIAL	THERMAL COND. K (w/cm - c°)	THERMAL DIFF. α (cm^2/sec)	TRANSITION TEMP. Tr (c°)
SAE 1045	0.36	0.068	790
SAE 4140	0.31	0.049	780
SAE 4340	0.28	0.047	750
SAE 8620	0.28	0.050	840
HYTEN B3X	0.30 (est.)	0.049	760 (est.)

predicted in advance, using the improved calculator program discussed in Section 2.2.5 above. The results of the processing are given in Tables VII through XI.

In addition, adjacent and overlapping runs in the pattern shown in Figure 8, were made on samples of SAE 8620 and Hyten B 3X. The results of these runs are shown in Figures 9 through 16. The hardness profiles shown in these figures were not obtained by surface hardness measurements, but by micro-hardness measurements taken 10 mils below the surface on samples cut normal to the processing direction.

2.2.8. Discussion of Results

The overall correlation between calculated and measured case is in the range of ±20-30% average over the entire range of processing speed and power used. The results for low speed processing of SAE 4140 and SAE 4340 are generally in even better agreement with the calculated values. This is clearly an improvement upon the results obtained in the preliminary survey.

- The values of the thermophysical constants used appear to be about right, with the exception of SAE 4340, where the value $\alpha = 0.047$ appears to be a little high.
- The surface hardness is somewhat low for most of the specimens, although full hardness is mostly achieved at $\sim$10 mils below the surface.

  This is not uncommon in laser hardening, and it has been suggested that this is due to a lower cooling rate at the surface. However, it is easy to demonstrate that this cannot in fact be the case, as the time for cooling from A_f to M_s is shorter at the surface than in the

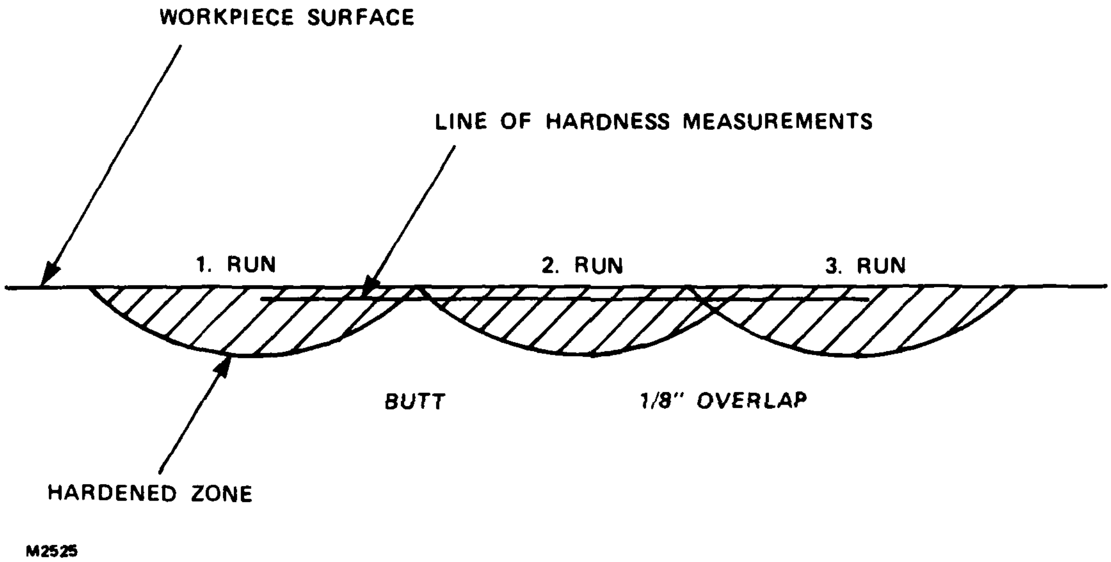

FIGURE 8 PROFILE OF OVERLAPPING RUNS

SAE 1045

95.7% OF THEORETICAL
STANDARD DEVIATION
20%

α = 0.068 cm^2/sec
T_T = 790° C

CONDITION	POWER (kW)	SPEED (in/min)	CALCULATED CASE (mil)	MEASURED CASE (mil)	% OF THEORETICAL	CALCULATED SURFACE TEMP. (C°)	SURFACE HARDNESS (Rc)
ANN	2.5	40	18.6	20	108	952	54.5
Q/T	2.5	40	18.6	21	113	952	56
H.R.	2.5	40	18.6	19	102	952	60
ANN	2.3	40	10.8	8	74	877	50
Q/T	2.3	40	10.8	13	120	877	52.5
H.R.	2.3	40	10.8	12	111	877	56
ANN	3.0	40	35.2	33.5	95	1139	57
Q/T	3.0	40	35.2	36	103	1139	56
H.R.	3.0	40	35.2	32	91	1139	59.5
ANN	2.5	30	36.6	24.5	67	1096	56
Q/T	2.5	30	36.6	28.5	78	1096	56
H.R.	2.5	30	36.6	31	85	1096	58
ANN	3.0	60	13.5	12.5	93	933	56
Q/T	3.0	60	13.5	13	96	933	54.5
H.R.	3.0	60	13.5	20.5	152	933	55
ANN	3.5	40	48.6	36.5	75	1325	56.5
Q/T	3.5	40	48.6	37.5	77	1325	57

100% OF THEORETICAL
STANDARD DEVIATION
28.6%

SAE 4140

$\alpha = 0.049\ cm^2/sec$
$T_T = 780°\ C$

CONDITION	POWER (kW)	SPEED (in/min)	CALCULATED CASE (mil)	MEASURED CASE (mil)	% OF THEORETICAL	CALCULATED SURFACE TEMP. (C°)	SURFACE HARDNESS (Rc)
ANN	2.3	40	8.9	12.5	140	865	52
Q/T	2.3	40	8.9	16.5	185	865	52
H.R.	2.3	40	8.9	6.0	67	865	48.5
ANN	2.3	30	23.7	16.5	70	996	57
Q/T	2.3	30	23.7	29.0	122	996	51.5
H.R.	2.3	30	23.7	16.5	70	996	52
ANN	1.4	15	13.8	17.5	127	860	53.5
Q/T	1.4	15	13.8	17.0	123	860	53.0
H.R.	1.4	15	13.8	12.5	91	860	51.5
ANN	1.6	15	31.4	22.5	72	980	52
Q/T	1.6	15	31.4	34.5	110	980	52.5
H.R.	1.6	15	31.4	22.5	72	980	52
ANN	1.7	15	39.1	32	82	1040	55.5
Q/T	1.7	15	39.1	43.5	111	1040	52
H.R.	1.7	15	39.1	34.5	88	1040	54
ANN	3.1	60	13.5	15	111	950	53.5
Q/T	3.1	60	13.5	18.5	137	950	51.5
H.R.	3.1	60	13.5	9	67	950	51.5
ANN	2.0	10	76.2	71	93	1306	53.5
Q/T	2.0	10	76.2	84.5	111	1306	52
H.R.	2.0	10	76.2	55.5	73	1306	54
ANN	1.7	5	103.7	102.5	99	1371	56.5
Q/T	1.7	5	103.7	83.5	81	1371	52.5
H.R.	1.7	5	103.7	105	101	1371	52

SAE 4340

90.2% OF THEORETICAL
STANDARD DEVIATION
23.3%

$\alpha = 0.047\ cm^2/sec$

$T_T = 750°\ C$

CONDITION	POWER (kW)	SPEED (in/min)	CALCULATED CASE (mil)	MEASURED CASE (mil)	% OF THEORETICAL	CALCULATED SURFACE TEMP. (C°)	SURFACE HARDNESS (Rc)
ANN	2.2	40	14.8	21.5	145	897	54
Q/T	2.2	40	14.8	13	88	897	53.5
H.R.	2.2	40	14.8	7	47	897	47.5
ANN	2.9	40	35.5	44	124	1176	55
Q/T	2.9	40	35.5	33	93	1176	54.5
H.R.	2.9	40	35.5	31	87	1176	52
ANN	2.3	40	33.5	32.5	97	1078	53
Q/T	2.3	40	33.5	26	78	1078	57
H.R.	2.3	40	33.5	23	69	1078	53.5
ANN	1.5	15	37.8	29	77	996	55
Q/T	1.5	15	37.8	25.5	67	996	53
H.R.	1.5	15	37.8	28.5	75	996	51.5
ANN	1.7	15	52.9	53	100	1126	54
Q/T	1.7	15	52.9	34	64	1126	54
H.R.	1.7	15	52.9	42	79	1126	51
ANN	2.8	60	14.6	22	151	931	54.5
Q/T	2.8	60	14.6	13	89	931	51.5
H.R.	2.8	60	14.6	12.5	86	931	52.5
ANN	1.9	10	86.1	83.5	97	1353	53.5
Q/T	1.9	10	86.1	73	85	1353	50.5
H.R.	1.9	10	86.1	72	84	1353	51
ANN	1.4	5	91.0	104	114	1238	53
Q/T	1.4	5	91.0	71.5	79	1238	51.5
H.R.	1.4	5	91.0	81.5	90	1238	49.5

95.5% OF THEORETICAL
STANDARD DEVIATION
29.0%

SAE 8620

α = 0.05 cm^2/sec

T_T = 840° C

CONDITION	POWER (kW)	SPEED (in/min)	CALCULATED CASE (mil)	MEASURED CASE (mil)	% OF THEORETICAL	CALCULATED SURFACE TEMP. (C°)	SURFACE HARDNESS (Rc)
Q/T	2.3	40	12	15	125	965	41
ANN	2.3	40	12	7	58	965	45
Q/T	2.0	30	14.2	21	148	969	41
ANN	2.0	30	14.2	12.5	88	969	38
Q/T	2.4	30	30.9	33	107	1159	40
ANN	2.4	30	30.9	31	100	1159	46.5
Q/T	1.6	15	36.3	34	94	1094	39
ANN	1.6	15	36.3	23	63	1094	44.5
Q/T	1.4	5	74.7	67.5	90	1258	41.5
ANN	1.4.	5	74.7	63.5	85	1258	43.5
Q/T	2.9	60	11.7	16	137	993	40.5
ANN	2.9	60	11.7	6	51	993	37.5

HYTEN B 3X

102.5% OF THEORETICAL
STANDARD DEVIATION
25.9%

$\alpha = 0.049\ cm^2/sec$
$T_T = 760°\ C$

CONDITION	POWER (kW)	SPEED (in/min)	CALCULATED CASE (mil)	MEASURED CASE (mil)	% OF THEORETICAL	CALCULATED SURFACE TEMP. (C°)	SURFACE HARDNESS (Rc)
Q/T	2.8	60	10.8	13	120	888	56.5
ANN	2.8	60	10.8	6	56	888	55.5
Q/T	2.2	40	10.2	15	147	855	57
ANN	2.2	40	10.2	11	108	855	55
Q/T	2.8	40	29.1	32	110	1083	57
ANN	2.8	40	29.1	33	113	1083	57.5
Q/T	3.5	40	45.4	44.5	98	1349	57.5
ANN	3.5	40	45.4	43.5	96	1349	58
Q/T	2.9	30	48.8	44	90	1242	56
ANN	2.9	30	48.8	43	88	1242	56.6

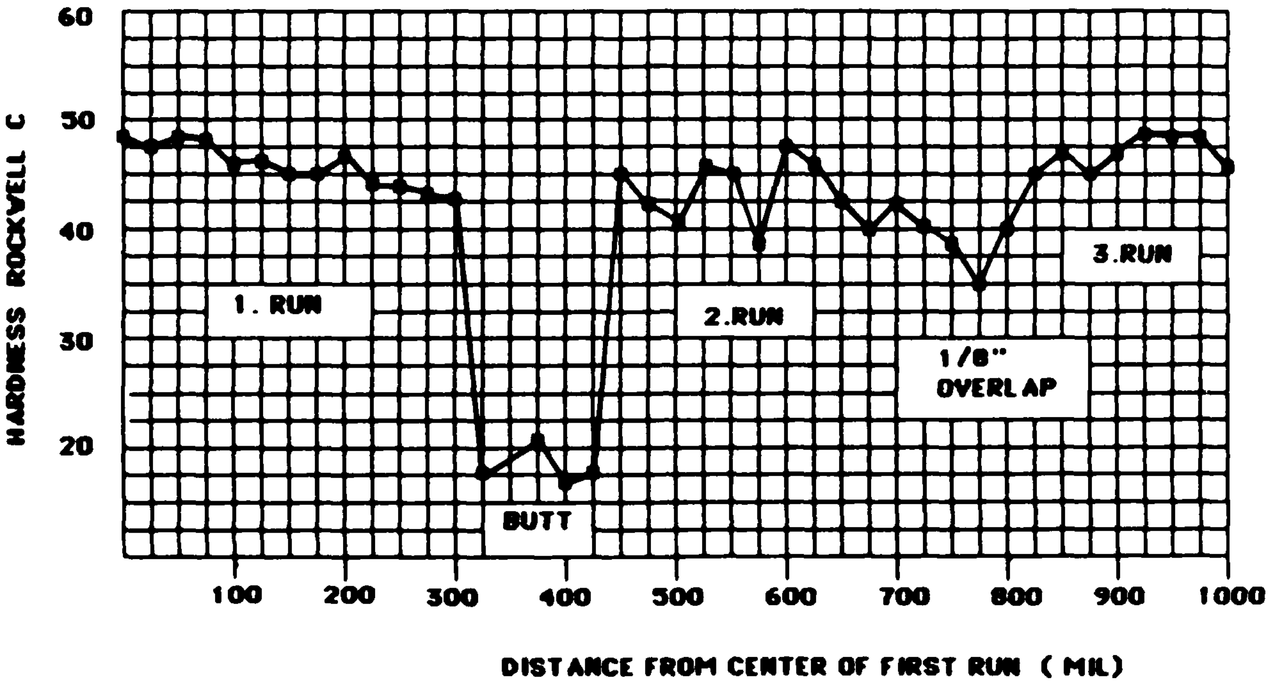

FIGURE 9.

SAE 8620 (HOT ROLLED). LASER HARDENED AT 1.4 Kw
AND 5 IN/MIN PROCESSING SPEED.

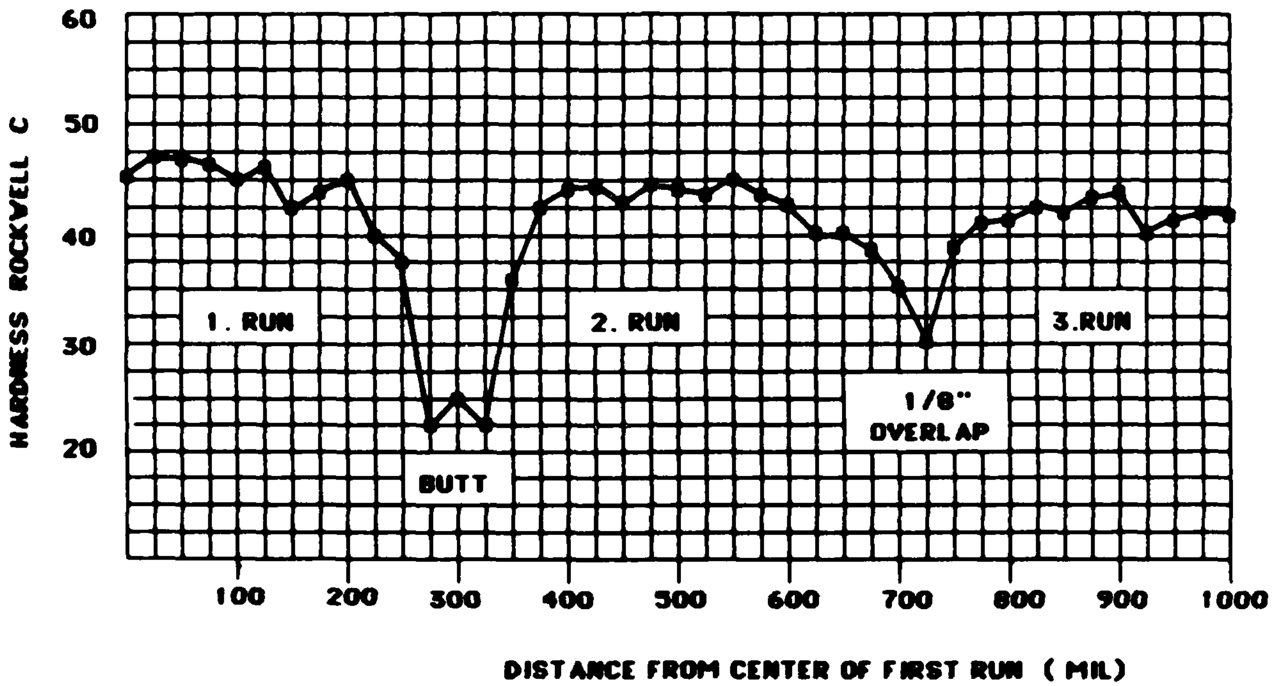

FIGURE 10.

SAE 8620 (QUENCHED AND TEMPERED). LASER HARDENED
AT 1.4 Kw AND 5 IN/MIN PROCESSING SPEED.

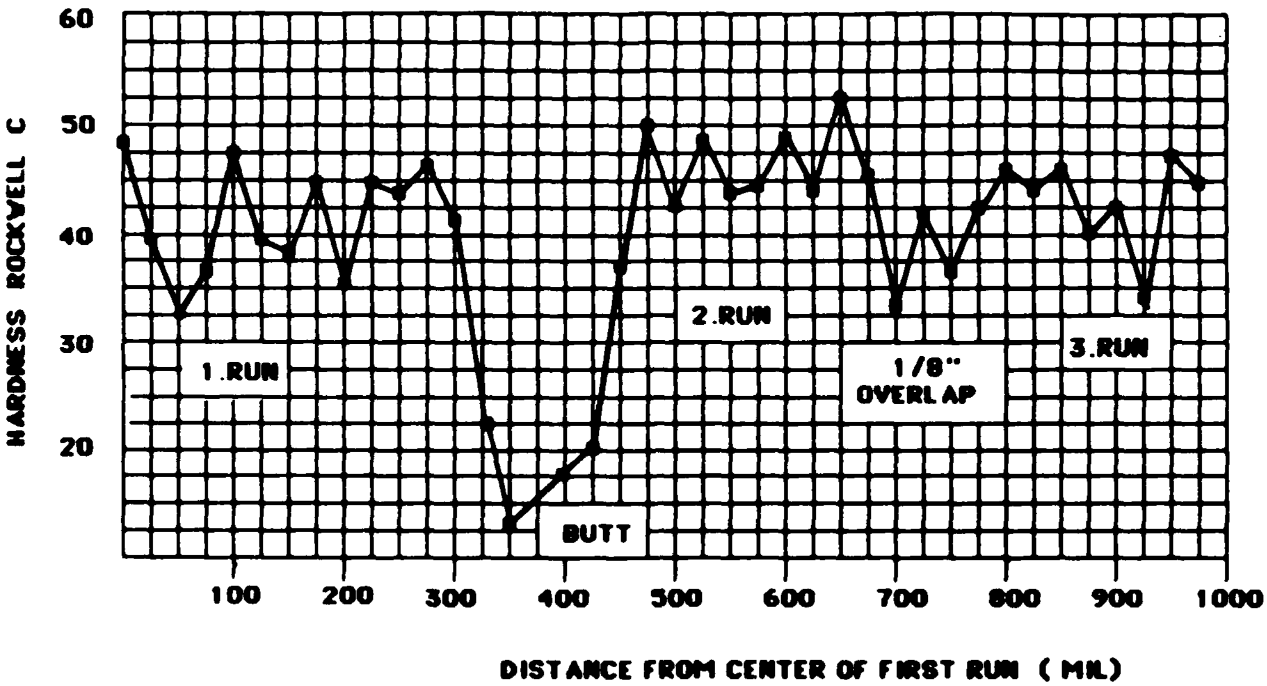

FIGURE 11.

SAE 8620 (HOT ROLLED). LASER HARDENED AT 2.4 Kw
AND 30 IN/MIN PROCESSING SPEED.

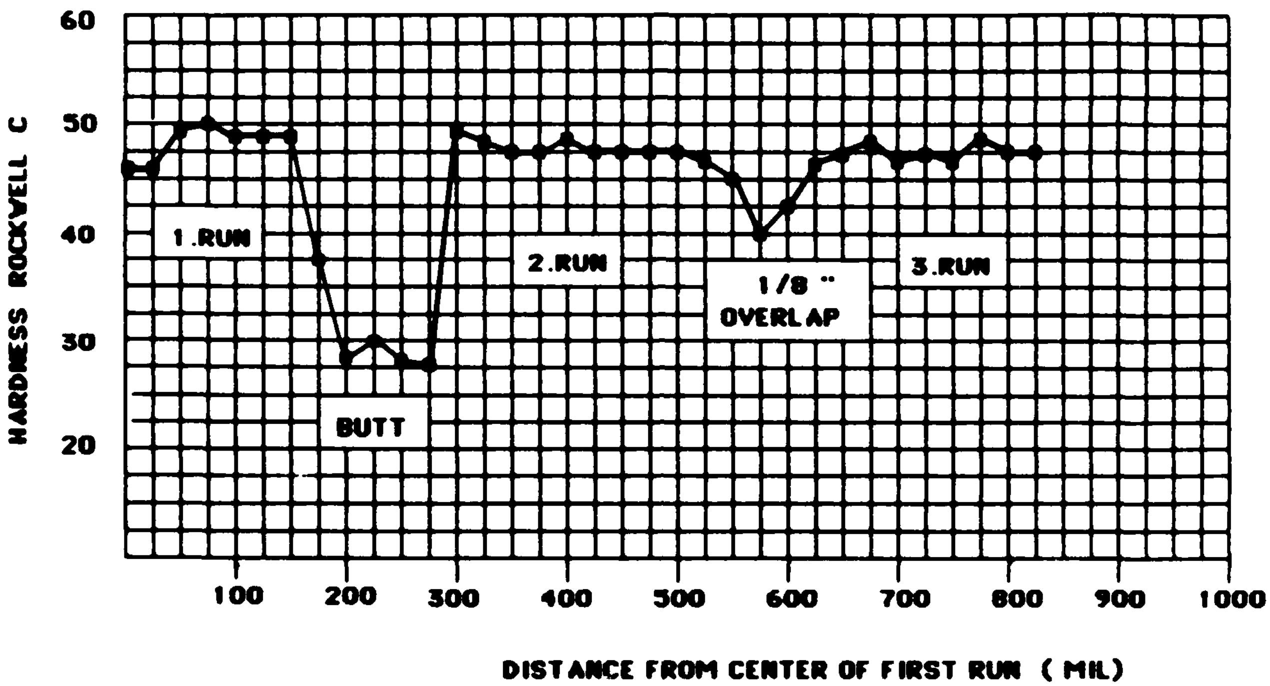

FIGURE 12.

SAE 8620 (QUENCHED AND TEMPERED). LASER HARDENED
AT 2.4 Kw AND 30 IN/MIN PROCESSING SPEED.

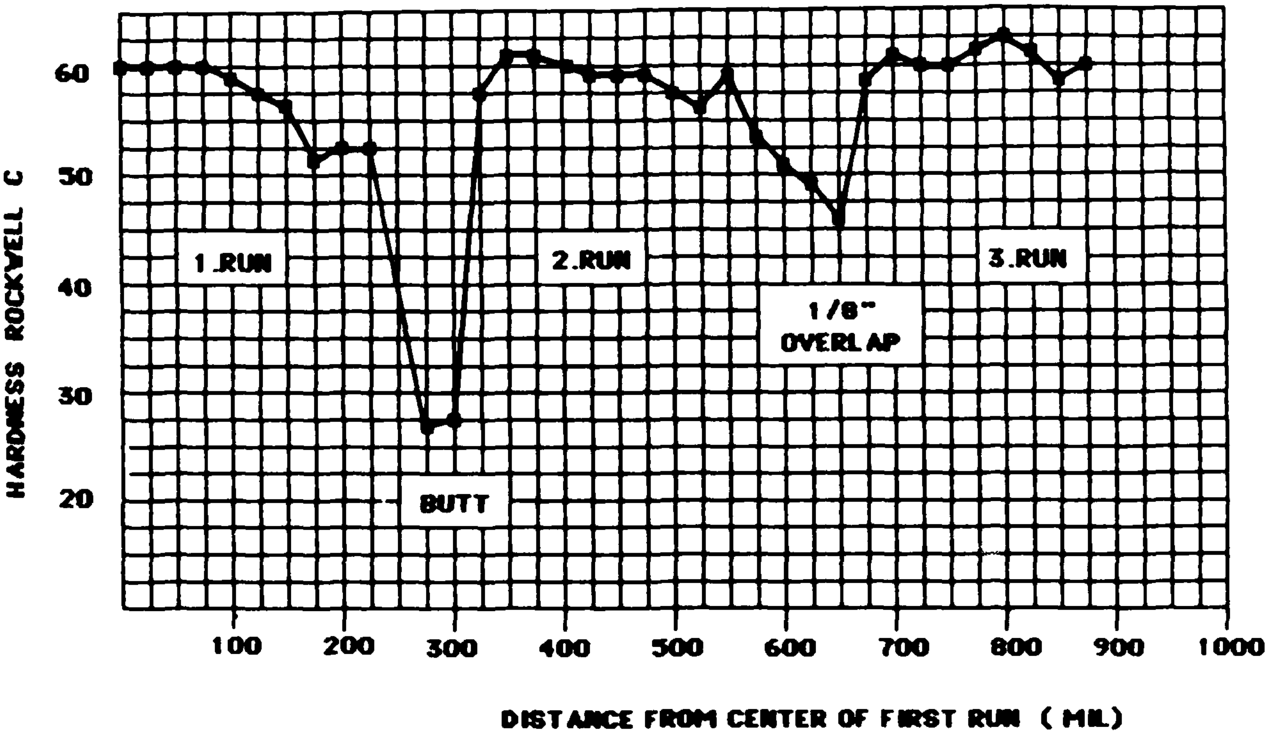

FIGURE 13.

HYTEN B 3X (QUENCHED AND TEMPERED). LASER HARDENED AT 1.2 Kw AND 5 IN/MIN PROCESSING SPEED.

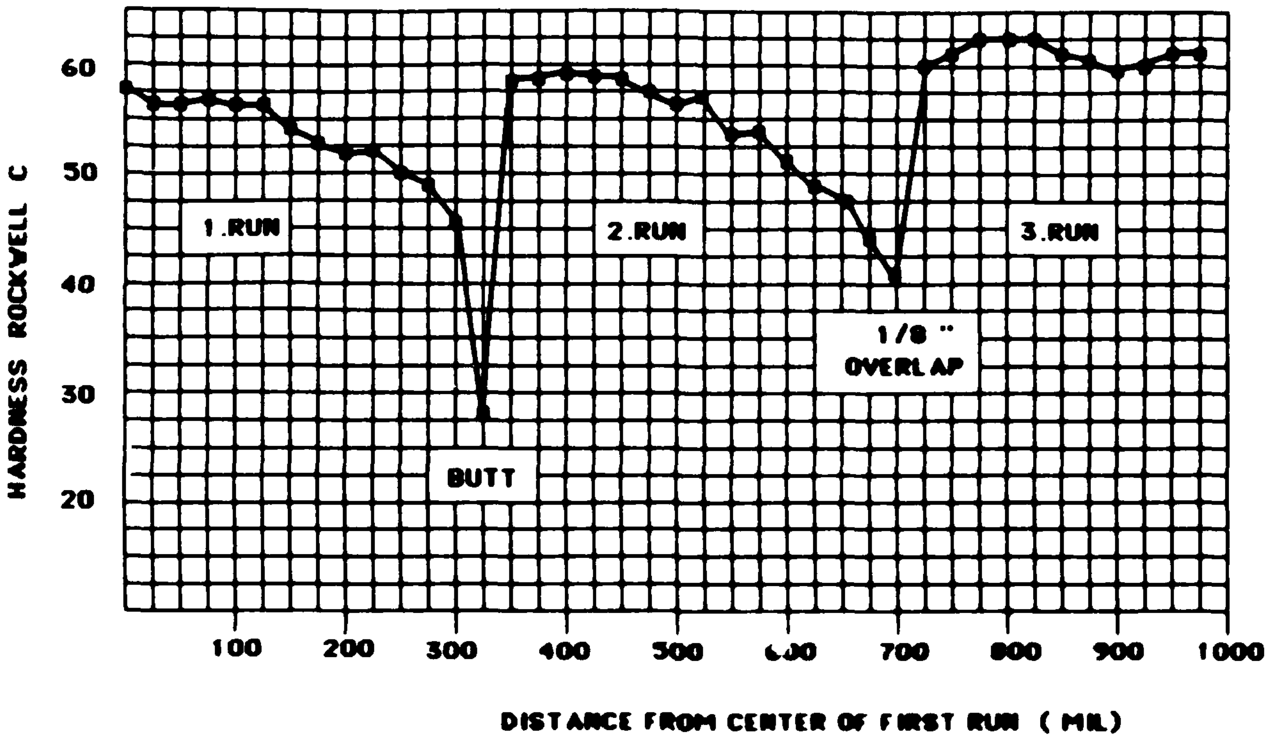

FIGURE 14

HYTEN B 3X (QUENCHED AND TEMPERED). LASER HARDENED
AT 1.6 Kw AND 5 IN/MIN PROCESSING SPEED.

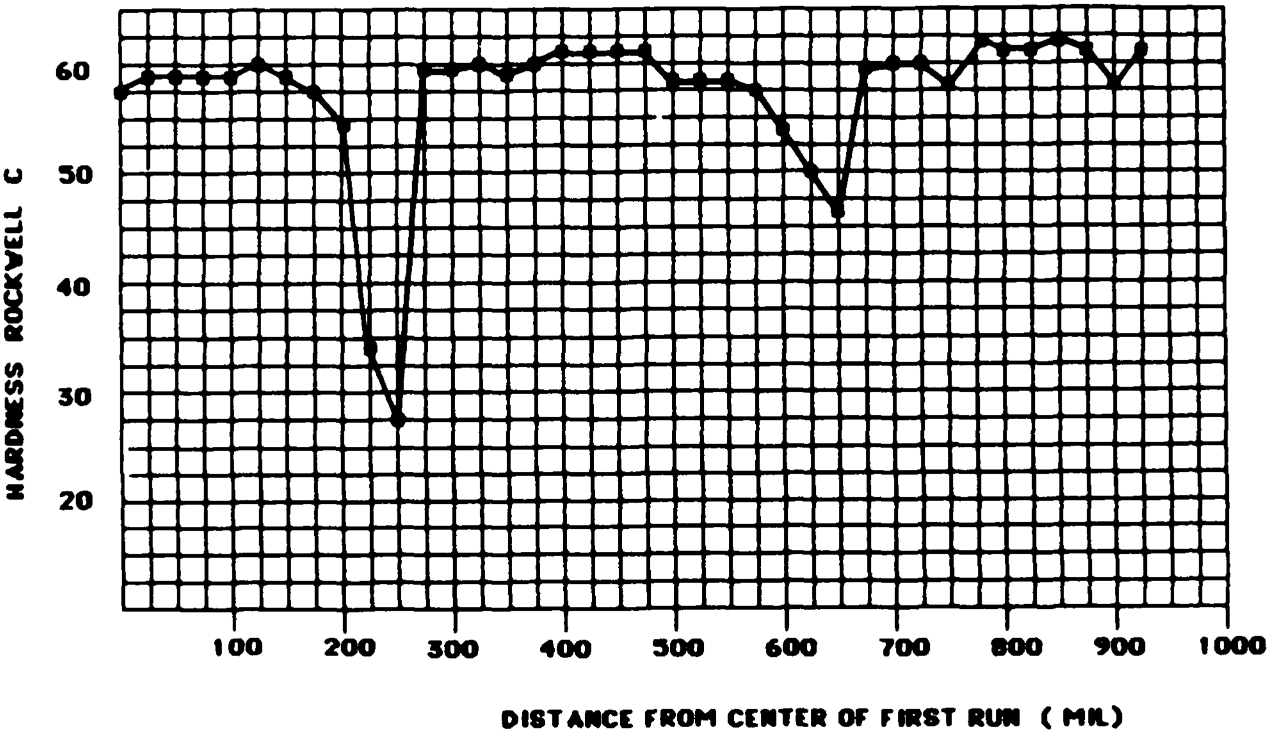

FIGURE 15.

HYTEN B 3X (QUENCHED AND TEMPERED).LASER HARDENED AT 2.9 Kw AT 30 IN/MIN PROCESSING SPEED.

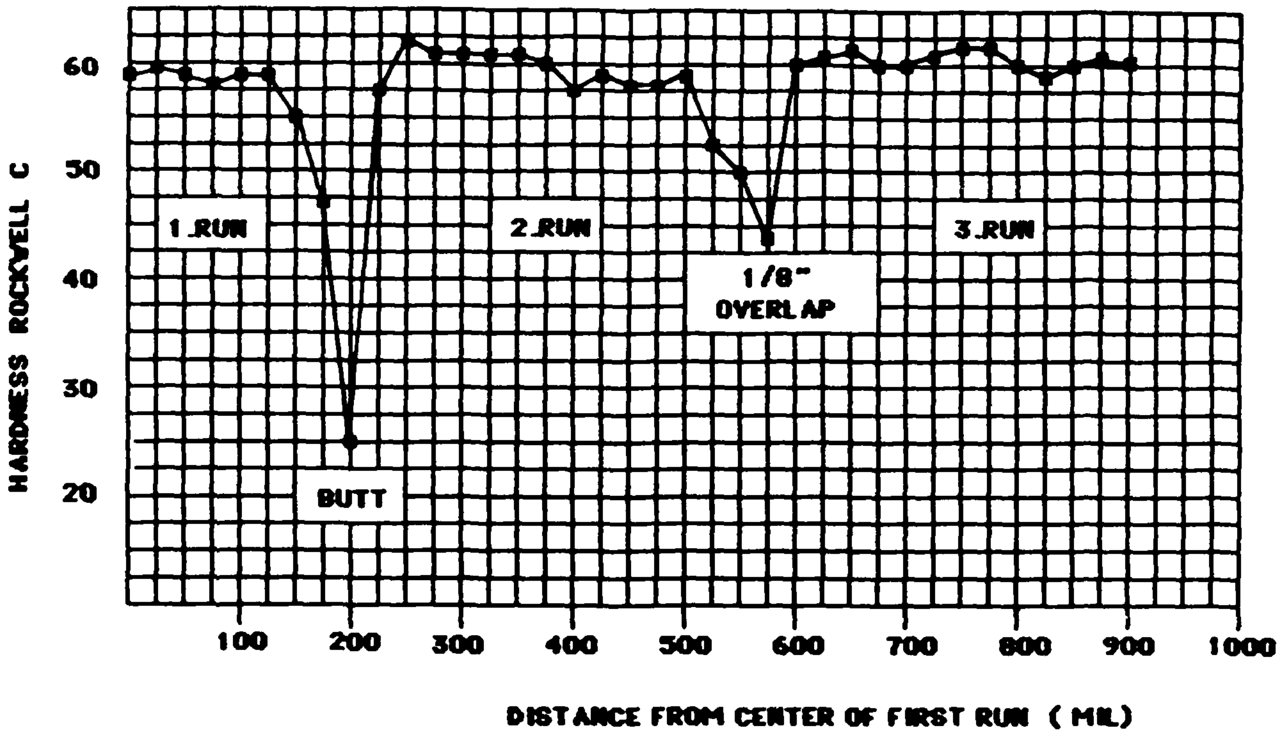

FIGURE 16.

HYTEN B 3X (QUENCHED AND TEMPERED). LASER HARDENED AT 2.9 Kw AND 40 IN/MIN PROCESSING SPEED.

interior. It is, however, possible that the surface will tend to contain a higher percentage of retained austenite than the interior, due to the very high temperature reached here during the laser processing. If this is the case, one should perhaps expect a more pronounced softening at low speed/high surface temperature, but this effect may be counteracted by the lower cooling rate occurrence in such cases. An answer to this question could, however, easily be obtained by X ray analysis.

- Overlap results show that positive overlap results in backtempering, but not to the bulk hardness of the material. From the point of view of hardness only, it is clearly more efficient to run overlap rather than butt to butt.

The 1020 samples provided by FMC did not develop an adequate hardened case under any combination of speed and power. From metallographic examination, it appeared that a slight decarburization had occurred at the surface, but removal of 50 mil of material by milling did not improve the hardenability of the material. A 1020 sample from Avco stock was processed for comparison purposes, and this material did harden, as expected. Figure 17 shows the hardness tracks obtained on these two materials at 2.9 kW power and 30 in/min speed. Figures 18 and 19 show the microstructure of the two materials. It is apparent that the grain size of the two materials is different, the FMC sample having the larger grain size; while there appears to be little difference in carbon content between the two. It is, therefore, reasonable to assume that the interaction time available in laser processing ($\sim$1 sec) is not sufficiently long to allow

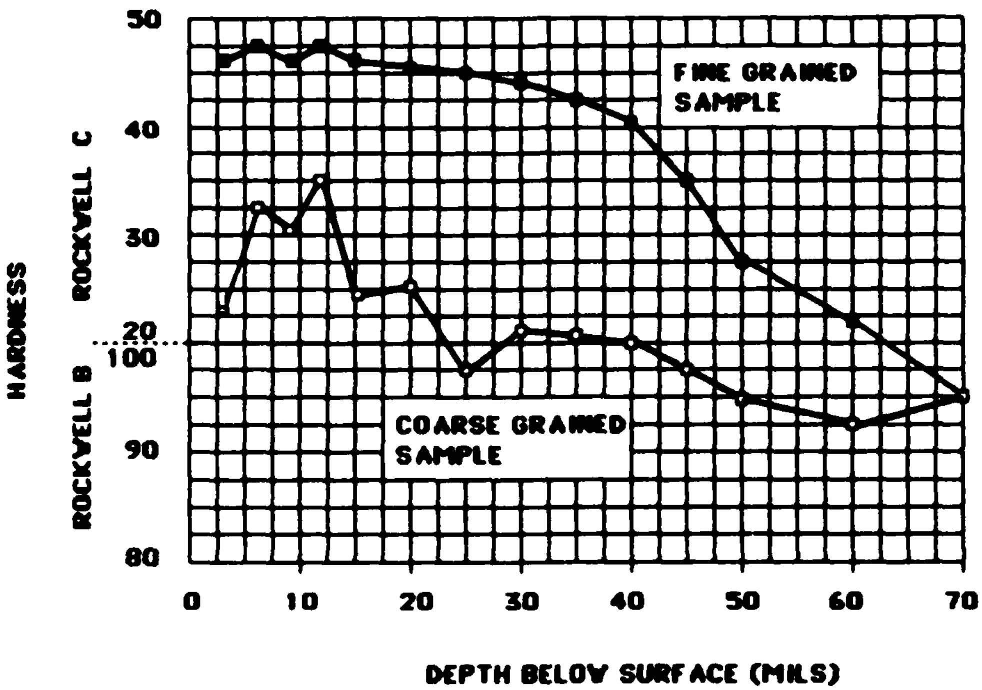

FIGURE 17.

HARDNESS PROFILES IN SAE 1020 STEELS, LASER HARDENED AT 2.9 Kw AND 30 IN/MIN PROCESSING SPEED.

FIGURE 18 STRUCTURE OF SAE 1020 (FMC)
500X

FIGURE 19 STRUCTURE OF SAE 1020 (AVCO)
500X

solution and redistribution of the carbon in the γ-phase to form a hardenable austenite in the coarse-grained material. Increased interaction time would give the longer carbon diffusion distances required for the coarse grained sample, but due to the low hardenability of 1020, the resulting self-quenching rates would not be sufficiently high to form 100% martensite. A profiled laser beam with "hot" leading edge would yield better results, but such a device was not available for this work.

The 4130 samples could not be laser processed with any benefit, since these samples already were in the fully hardened, untempered condition. (Bulk Hardness Rc 51). The only results of the laser processing are some softening at the surface, and tempering of the material at the bottom of the heat-affected zone.

3. CLADDING OF CATAPULT RAIL BARS

3.1 Objective

The objective of this phase of the program was to determine the feasibility of laser cladding carrier catapult rails with wear-resistant alloys, and to develop preliminary processing parameters and procedures for such cladding. Specifically, it was desired to develop methods for cladding the rail material with hardfacing alloys having approximately the same hardness as the substrate (approximately Rockwell C 32). Furthermore, the cladding process should be such that sharp edges could be maintained on the finished product. The final objective was to produce representative samples of cladded rail sections.

3.2 Experimental Work

3.2.1. Materials

Sample rails of two different types were provided by FMC/NOD. These consisted of bars made from SAE 4140 and Hy-90 steel, having cross-sectional dimensions 1 1/2" x 2". Two of the rail samples had been flame-sprayed with Stellite #6 E on one face. The other rails were uncoated.

For the laser cladding of the rails, three different types of hardfacing powder were provided. These consisted of Deloro 22, Deloro 35 and Stellite #6 E. In addition, 304 stainless steel powder for dilution of the hardfacing alloys was provided, in order to allow control of the cladding hardness and to lower cracking susceptibility where needed.

3.2.2. Equipment and Procedures

The laser processing was performed with an Avco HPL®-10 CO_2 laser with CW output. The laser output beam was shaped with a square beam by means of an optical integrator, as shown in Figure 1. This beam had dimensions 1/2" x 1/2" in the focal plane. The entire experimental arrangement was essentially identical to the setup used for the heat treatment work discussed in Chapter 2 in this report and shown in Figure 2, with the addition of an argon gas blanket nozzle aimed at the laser spot from the trailing edge side of the spot.

The object of this gas blanket was to protect the molten material in the interaction zone from reaction with the ambient atmosphere. The gas flow through the nozzle was 15 fe^3/hr.

The alloy powder was preplaced onto the substrate surface, using 1/16" thick templates to obtain even coverage. Originally, it was the intention to use an automatic powder feeder for delivery of the alloy powder to the substrate, but the alloy powder used in this work did not flow well through this feeder. In particular, the stainless steel powder created problems due to its small grain size (+ 10 μm).

3.2.3. Development of Processing Parameters

Trial runs were made with all three powders at various power levels and processing speeds, ranging from 3 kW/cm^2 to 6 kW/cm^2 and 0.211 cm/sec to 0.847 cm/sec (5 in/min to 20 in/min). Both straight alloy powders and alloy powders with various amounts of 304 stainless steel powder added were clad onto 1/2" SAE 4140 steel plates.

It quickly became clear that the Stellite powder needed about 40% stainless steel addition, both to prevent cracking and to lower the hardness to an acceptable level. At this stage, no cracking problem was experienced with Deloro 22 and Deloro 35. However, stainless steel addition to these two alloys resulted in a clad layer with variable hardness.

Because of this, it was decided to process the two Deloro alloys without stainless steel addition, even though the resulting clad layer had a hardness somewhat in excess of Rockwell C 32.

The following processing parameters gave the best combination of smooth flow, minimal dilution with the substrate, and absence of porosity.

<u>STELLITE #6 E + 40% STAINLESS STEEL</u>

4.65 kW/cm^2	10 in/min

<u>DELORO 22</u>

4.65 kW/cm^2	8 in/min

<u>DELORO 35</u>

4.65 kW/cm^2	10 in/min

Following the determination of the optimal processessing parameters, overlapping runs were made (1/8" overlap). No problems with cracking or flow were encountered at this stage, but a tendency for pore formation in the Deloro 35 specimens in the overlap zone was noticed. These pores were predominantly in the surface region and did not appear to be of critical importance.

Finally, processing of the flame-sprayed test bars was attempted. This was not a success because the only effect of the laser processing, over a wide range of power and speed, was erosion of the sprayed layer. At power input rates sufficiently high to cause any reaction whatsoever, a veritable shower of sparks was generated. This gave the impression that the sprayed layer was under intense residual stresses.

3.2.4. Edge Control

In order to obtain sharp edges on the clad bars, both at the ends and along the edges, a series of runs were made to find a way to obtain this. The following techniques were found to give satisfactory results.

- To obtain sharp edges at the ends of the bars, two short pieces were cut from the barstock and used as run-on and run-off pieces. The fitup of these pieces must be good enough to allow cladding across the gap without any loss of powder through the gap. If necessary, the gap could be sealed off with a slurry of the alloy powder. (Alcohol or Nicobraze can be used as a carrier). By starting the cladding at least an inch past the end-gap, a continuous clad deposit could be made. After laser processing, the end-pieces could be knocked off cleanly, or cut by sawing or abrasive wheel.

- To obtain sharp edges along the bar, stainless steel extension surfaces were used. These consisted of 1/16" stainless (304) plates fitting tightly along the edges. These plates were clamped down on another steel bar to provide heat-sinking. It is important that the extension surface is as long as the bar plus the two end pieces, otherwise through-melting will result at the corners. The edge cladding was performed with about half the width of the final run on the bar and the other half on the extension surface. After processing, the stainless steel plate could be cut from the underside, providing a sharp edge. Figure 20 shows the technique of edge control.

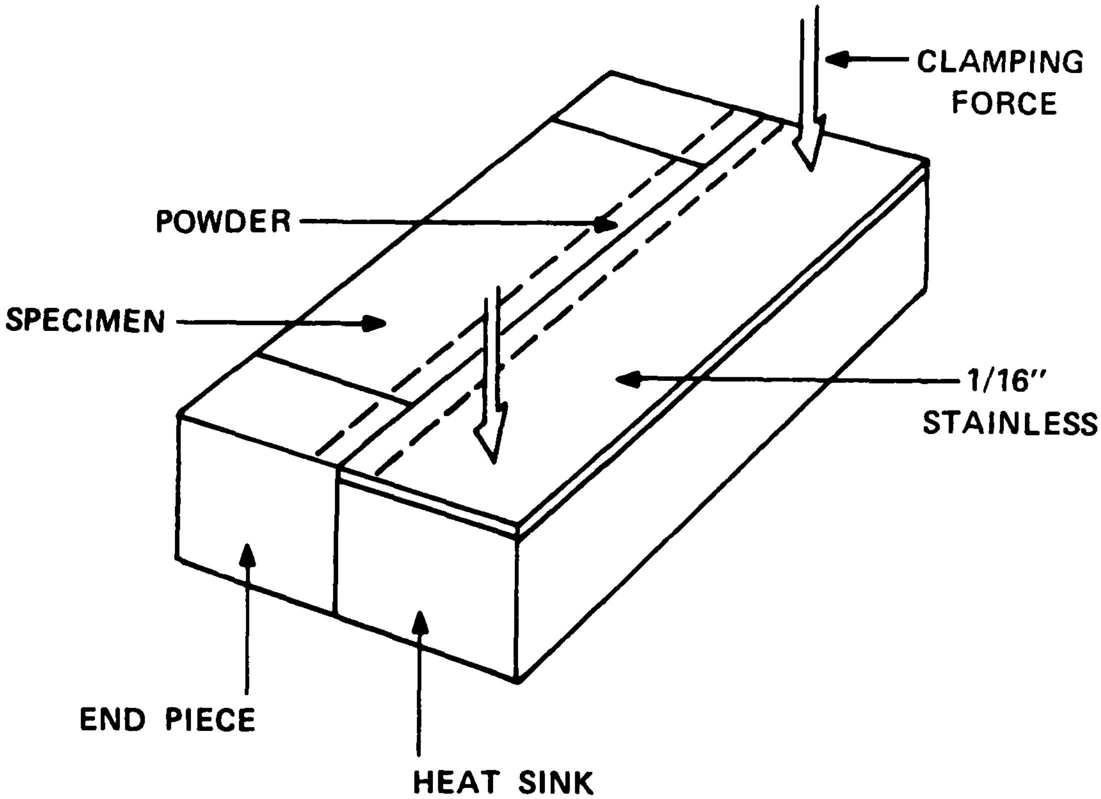

L4241

FIGURE 20 EDGE CONTROL IN LASER CLADDING

3.2.5. Preparation of Specimens

Six specimens, each about 2.5" long, were cut from the 1 1/2" x 2" bars, three from SAE 4140 bars and three from Hy-90 bars. These were clad on one of the 1 1/2" faces, using overlapping runs and edge control techniques (as described above) to obtain uniform cladding of about 0.05" thickness over the entire surface. Each of the three alloys were clad onto both SAE 4140 and Hy-90 substrates. Figure 21 shows the shape of the final specimens. (Deloro 22 on SAE 4140).

3.3 Results and Discussion

Both the Stellite #6 E + 40% stainless steel specimens developed cracks at the third overlay pass. These cracks were of the "herring bone" type. The Deloro 35 specimens also showed cracks in the third overlay, but these were normal to the processing direction. In order to prevent cracking, new specimens were made as before, but with stress relief between each cladding run (1200°F for 1 hour). No improvement was observed in the Stellite #6 E specimens, but one of the Deloro 35 (on SAE 4140) was apparently crack-free. Deloro 35 on Hy-90, however, showed the cracks.

The two Deloro 22 specimens showed no cracks, and these were not stress-relieved between runs.

Figures 22 through 24 show the hardness profiles of the six different cladded specimens. In all cases, the clad layer is 45 to 50 mil deep, with a hardness ranging from 32 to 42 Rockwell C. The substrates of the specimens cladded with Deloro 22 show transformation hardening in the vicinity of the clad/substrate interface. This is absent in the other specimens, due to the stress-relief heat treatment.

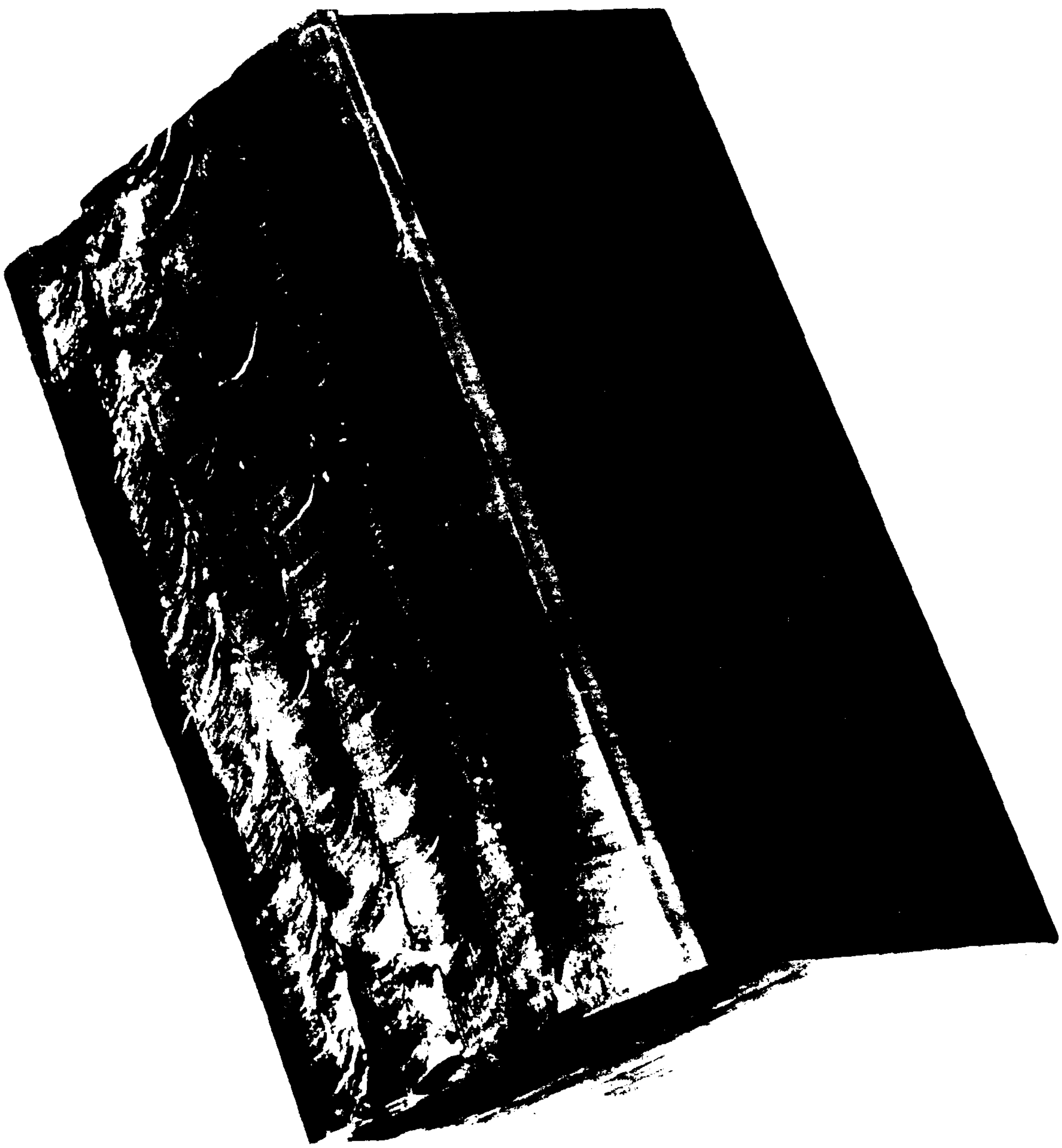

FIGURE 21 SAE 4140 STEEL BAR CLADDED WITH DELORO 22

Cladding of catapult rails with Deloro 22 can be performed easily. The hardness of the overlay is Rockwell C 35 to 40. The 4140 substrate shows transformation hardening to a peak hardness of Rc 51-52. The Hy-90 substrate does not harden to more than Rc 40.

The Deloro 35 and Stellite #6 E alloys can probably not be clad onto these steels in a continuous manner without preheating and slow post-processing cooling to prevent cracking.

Remelting of flame-sprayed layers was not successful in this case, but this should be possible if closer control of the spraying process is exercised.

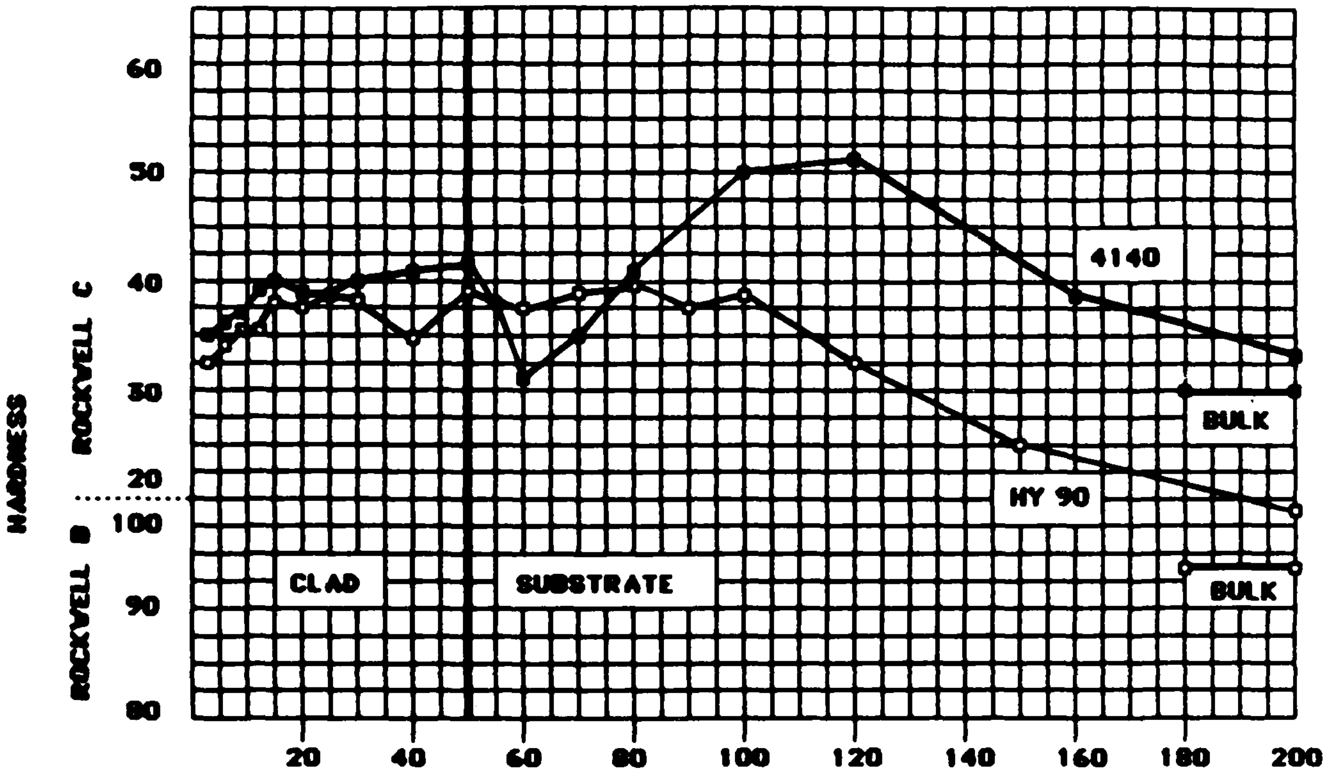

FIGURE 22.

DELORO 22. LASER CLADDED AT 4.65 Kw/cm^2
AND 0.339 cm/sec PROCESSING SPEED.

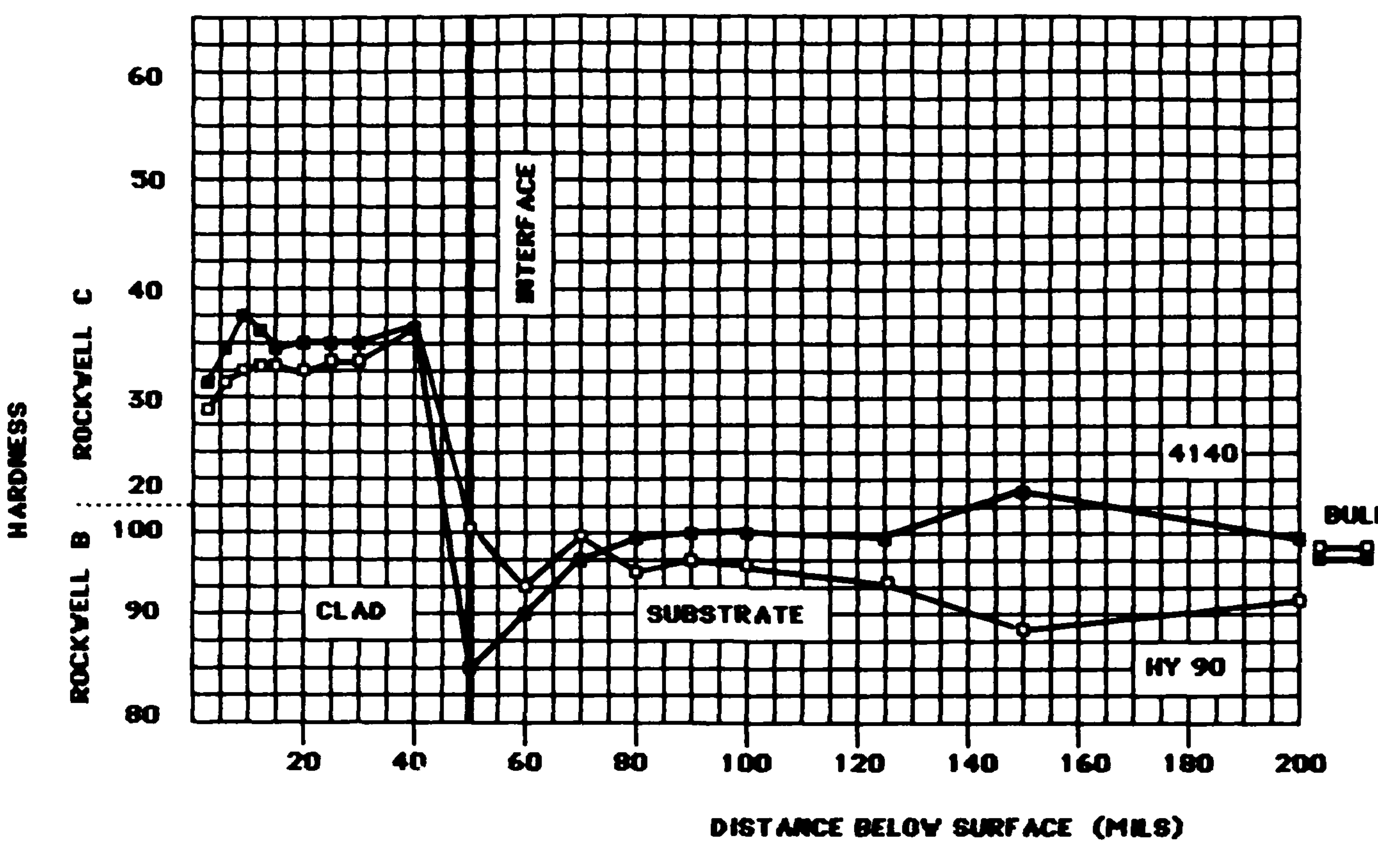

FIGURE 23

STELLITE 6 E + 40% STAINLESS STEEL, LASER CLADDED
AT 4.65 Kw/cm^2 AND 0.423 cm/sec PROCESSING SPEED.

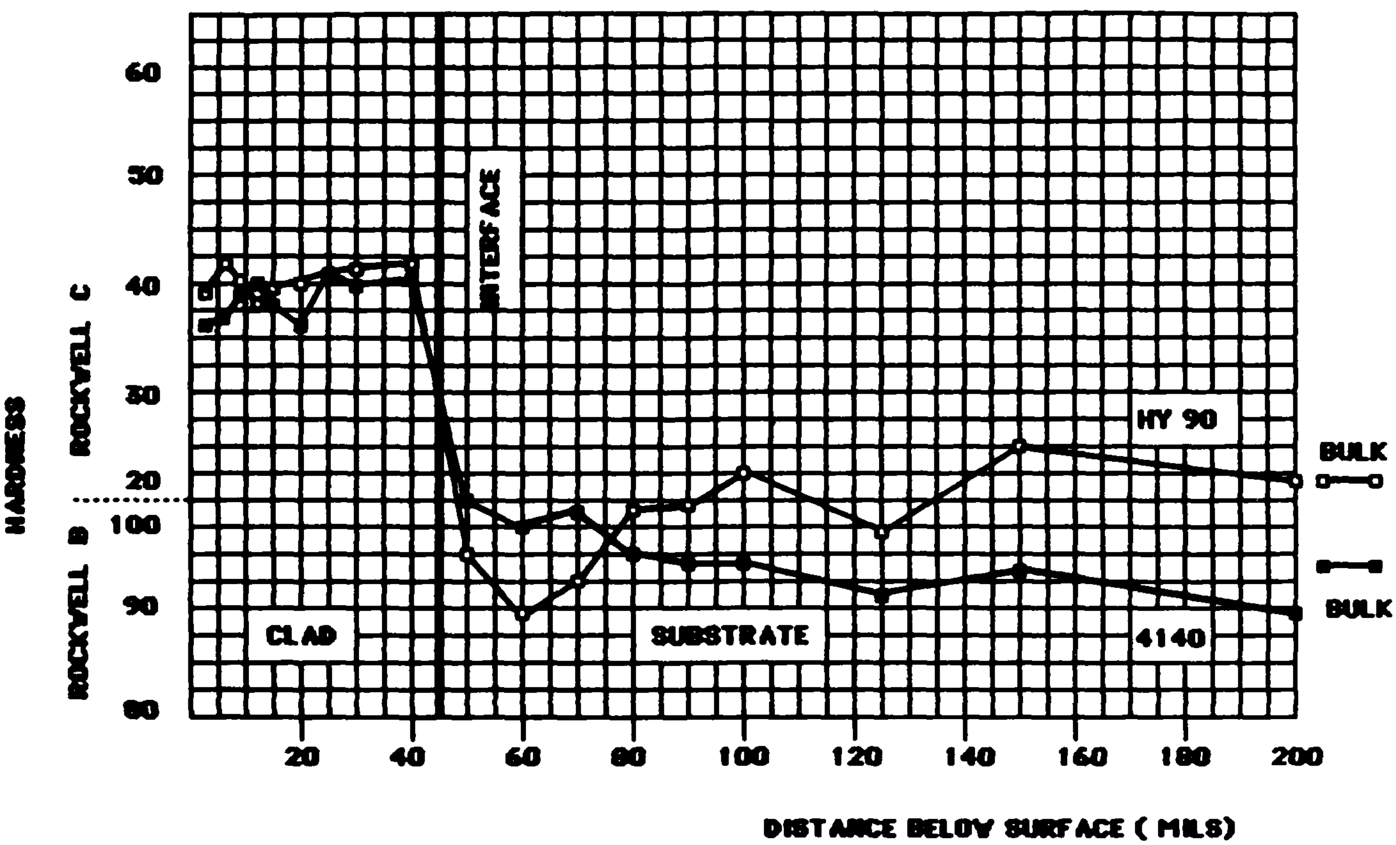

FIGURE 24.

DELORO 35. LASER CLADDED AT 4.65 Kw/cm^2
AND 0.423 cm/sec PROCESSING SPEED.

LIST OF REFERENCES

1) Rose, A., and Strassburg, V. (1956). Stahl and Eisen, 76, No. 15. 976-983.

2) Sandven, O.A. (1981). Laser Surface Heat Treatment With Profiled Beams. Proc. International Laser Conf., Anaheim, CA.

3) Carslaw, H.S. and Jaeger, J.C. (1959). Conduction of Heat in Solids. Oxford Press, 2nd ed. 75.

4) ibid. 270.

5) Sandven, O.A. (1983). Three-Dimensional Heat Flow Model for Prediction of Case Depth in Laser Surface Transformation Hardening. ICALEO Conf., Los Angeles, CA.

6) ASM METALS HANDBOOK, 9th Ed. (1978). Vol. 1: 145-151.

APPENDIX I

The program listed on the following pages is based on the one-dimensional heat flow model and should not be used for low processing speed.

The program is written for use on a Texas Instrument TI 59 programmable calculator with a PC-100C printer.

User Instructions

1. Partition the calculator to mode 714:29 by entering 3 and push 2th op. 17.
2. Enter power density in A (w/cm^2).
3. Enter speed in B (cm/sec).
4. Enter spot length in C (cm).
5. Enter thermal conductivity and press R/S (w/cmC°).
6. Enter thermal diffusivity and press R/S (cm^2/sec).
7. Enter room temperature in D (C°).
8. Enter transition temperature and press R/S (c°).
9. Execute program by pressing A^1.

The calculator will print dwelltime, surface temperature and case depth. If the heat input is insufficient to form any case, "NO CASE" is printed. If the processing speed is too low for this model, "USE 3-D" will be printed.

If cooling rates behind the laser spot are desired, enter the total time (dwelltime + cooling time combined) and press B^1. This must be done after the case depth has been calculated. The calculator will print surface temperature at the entered time, the rate of cooling (in c°/sec), the temperature at the bottom of the case and the rate of cooling at this point. The procedure can be repeated for any desired total time.

PROGRAM FOR PREDICTION OF CASE DEPTH
(One-Dimensional)

```
000  76  LBL
001  11   A
002  53   (
003  42  STO
004  00   00
005  65   ×
006  00   0
007  93   .
008  08   8
009  05   5
010  95   =
011  42  STO
012  10   10
013  54   )
014  92  RTN
015  76  LBL
016  12   B
017  53   (
018  42  STO
019  01   01
020  54   )
021  92  RTN
022  76  LBL
023  13   C
024  53   (
025  42  STO
026  02   02
027  91  R/S
028  42  STO
029  03   03
030  91  R/S
031  42  STO
032  04   04
033  54   )
034  92  RTN
035  76  LBL
036  14   D
037  53   (
038  42  STO
039  05   05
040  91  R/S
041  42  STO
042  06   06
043  54   )
044  92  RTN
045  76  LBL
046  16   A'
047  53   (
048  43  RCL
049  02   02
050  55   ÷
051  43  RCL
052  01   01
053  95   =
054  42  STO
055  07   07
056  25  CLR
057  69  OP
058  00   00
059  01   1
060  06   6
061  04   4
062  03   3
063  01   1
064  07   7
065  02   2
066  07   7
067  02   2
068  07   7
069  69  OP
070  01   01
071  69  OP
072  05   05
073  43  RCL
074  07   07
075  99  PRT
076  01   1
077  06   6
078  65   ×
079  43  RCL
080  04   04
081  55   ÷
082  43  RCL
083  01   01
084  95   =
085  32  X:T
086  43  RCL
087  02   02
088  77   GE
089  01   01
090  13   13
091  25  CLR
092  69  OP
093  00   00
094  04   4
095  01   1
096  03   3
097  06   6
098  01   1
099  07   7
100  69  OP
101  01   01
102  00   0
103  04   4
104  03   3
105  00   0
106  01   1
107  06   6
108  69  OP
109  02   02
110  69  OP
111  05   05
112  92  RTN
113  02   2
114  65   ×
115  43  RCL
116  10   10
117  55   ÷
118  43  RCL
119  03   03
120  65   ×
121  53   (
122  43  RCL
123  04   04
124  65   ×
125  43  RCL
126  07   07
127  55   ÷
128  89   π
129  54   )
130  34  √x
131  85   +
132  43  RCL
133  05   05
134  95   =
135  42  STO
136  08   08
137  43  RCL
138  06   06
139  32  X:T
140  43  RCL
141  08   08
142  77   GE
143  01   01
144  68   68
145  25  CLR
146  69  OP
147  00   00
148  03   3
149  01   1
150  0[illegible]   [illegible]
```

PROGRAM FOR PREDICTION OF CASE DEPTH
(One-Dimensional)

151	02	2	201	55	÷	251	65	×
152	69	OP	202	43	RCL	252	43	RCL
153	01	01	203	03	03	253	11	11
154	01	1	204	65	×	254	85	+
155	05	5	205	53	(	255	43	RCL
156	01	1	206	43	RCL	256	05	05
157	03	3	207	04	04	257	95	=
158	03	3	208	65	×	258	42	STO
159	06	6	209	43	RCL	259	15	15
160	01	1	210	07	07	260	43	RCL
161	07	7	211	54	)	261	15	15
162	69	OP	212	34	√X	262	75	-
163	02	02	213	95	=	263	43	RCL
164	69	OP	214	42	STO	264	06	06
165	05	05	215	11	11	265	95	=
166	54	)	216	02	2	266	50	I×I
167	92	RTN	217	65	×	267	32	X:T
168	25	CLR	218	53	(	268	01	1
169	69	OP	219	43	RCL	269	77	GE
170	00	00	220	04	04	270	03	03
171	03	3	221	65	×	271	31	31
172	06	6	222	43	RCL	272	43	RCL
173	04	4	223	07	07	273	06	06
174	01	1	224	54	)	274	32	X:T
175	03	3	225	34	√X	275	43	RCL
176	05	5	226	95	=	276	15	15
177	02	2	227	42	STO	277	77	GE
178	01	1	228	12	12	278	03	03
179	69	OP	229	00	0	279	14	14
180	01	01	230	42	STO	280	86	STF
181	03	3	231	13	13	281	01	01
182	07	7	232	00	0	282	43	RCL
183	01	1	233	93	.	283	14	14
184	07	7	234	00	0	284	55	÷
185	03	3	235	05	5	285	02	2
186	00	0	236	42	STO	286	95	=
187	03	3	237	14	14	287	42	STO
188	03	3	238	43	RCL	288	14	14
189	69	OP	239	13	13	289	43	RCL
190	02	02	240	85	+	290	13	13
191	69	OP	241	43	RCL	291	75	-
192	05	05	242	14	14	292	43	RCL
193	43	RCL	243	95	=	293	14	14
194	08	08	244	42	STO	294	95	=
195	59	INT	245	13	13	295	42	STO
196	99	PRT	246	55	÷	296	13	13
197	02	2	247	43	RCL	297	55	÷
198	65	×	248	12	12	298	43	RCL
199	43	RCL	249	95	=	299	12	12
200	10	10	250	10	E'	300	95	=

PROGRAM FOR PREDICTION OF CASE DEPTH

(One-Dimensional)

```
301   10  E'
302   65   x
303   43  RCL
304   11   11
305   85   +
306   43  RCL
307   05   05
308   95   =
309   42  STO
310   15   15
311   61  GTO
312   02   02
313   60   60
314   87  IFF
315   01   01
316   03   03
317   21   21
318   61  GTO
319   02   02
320   38   38
321   43  RCL
322   14   14
323   55   ÷
324   02   2
325   95   =
326   42  STO
327   14   14
328   61  GTO
329   02   02
330   38   38
331   25  CLR
332   69  OP
333   00   00
334   01   1
335   05   5
336   01   1
337   03   3
338   03   3
339   06   6
340   01   1
341   07   7
342   69  OP
343   01   01
344   69  OP
345   05   05
346   43  RCL
347   13   13
348   99  PRT
349   98  ADV
350   22  INV
351   86  STF
352   01   01
353   54   )
354   92  RTN
355   76  LBL
356   17  B'
357   53   (
358   42  STO
359   16   16
360   02   2
361   65   x
362   43  RCL
363   10   10
364   55   ÷
365   43  RCL
366   03   03
367   65   x
368   43  RCL
369   04   04
370   34  √X
371   95   =
372   42  STO
373   17   17
374   43  RCL
375   17   17
376   65   x
377   53   (
378   43  RCL
379   16   16
380   55   ÷
381   89   π
382   54   )
383   34  √X
384   95   =
385   42  STO
386   18   18
387   43  RCL
388   17   17
389   65   x
390   53   (
391   53   (
392   43  RCL
393   16   16
394   75   -
395   43  RCL
396   07   07
397   54   )
398   55   ÷
399   89   π
400   54   )
401   34  √X
402   95   =
403   42  STO
404   19   19
405   43  RCL
406   18   18
407   75   -
408   43  RCL
409   19   19
410   85   +
411   43  RCL
412   05   05
413   95   =
414   42  STO
415   20   20
416   59  INT
417   99  PRT
418   53   (
419   43  RCL
420   08   08
421   75   -
422   43  RCL
423   20   20
424   54   )
425   55   ÷
426   53   (
427   43  RCL
428   16   16
429   75   -
430   43  RCL
431   07   07
432   54   )
433   95   =
434   59  INT
435   99  PRT
436   43  RCL
437   13   13
438   55   ÷
439   02   2
440   55   ÷
441   53   (
442   43  RCL
443   04   04
444   65   x
445   43  RCL
446   16   16
447   54   )
448   34  √X
449   95   =
450   10  E'
```

PROGRAM FOR PREDICTION OF CASE DEPTH

(One-Dimensional)

```
451  65  ×
452  43  RCL
453  17   17
454  65  ×
455  43  RCL
456  16   16
457  34  √X
458  95  =
459  42  STO
460  21   21
461  43  RCL
462  13   13
463  55  ÷
464  02  2
465  55  ÷
466  53  (
467  43  RCL
468  04   04
469  65  ×
470  53  (
471  43  RCL
472  16   16
473  75  -
474  43  RCL
475  07   07
476  54  )
477  54  )
478  34  √X
479  95  =
480  10  E'
481  65  ×
482  43  RCL
483  17   17
484  65  ×
485  53  (
486  43  RCL
487  16   16
488  75  -
489  43  RCL
490  07   07
491  54  )
492  34  √X
493  95  =
494  42  STO
495  22   22
496  43  RCL
497  21   21
498  75  -
499  43  RCL
500  22   22
501  85  +
502  43  RCL
503  05   05
504  95  =
505  42  STO
506  23   23
507  59  INT
508  99  PRT
509  53  (
510  43  RCL
511  15   15
512  75  -
513  43  RCL
514  23   23
515  54  )
516  55  ÷
517  53  (
518  43  RCL
519  16   16
520  75  -
521  43  RCL
522  07   07
523  54  )
524  95  =
525  59  INT
526  99  PRT
527  54  )
528  92  RTN
529  76  LBL
530  10  E'
531  53  (
532  42  STO
533  24   24
534  04  4
535  32  X:T
536  43  RCL
537  24   24
538  77  GE
539  06   06
540  73   73
541  43  RCL
542  24   24
543  65  ×
544  00  0
545  93  .
546  03  3
547  02  2
548  07  7
549  05  5
550  09  9
551  01  1
552  01  1
553  85  +
554  01  1
555  95  =
556  35  1/X
557  42  STO
558  25   25
559  53  (
560  00  0
561  93  .
562  02  2
563  05  5
564  04  4
565  08  8
566  02  2
567  02  2
568  09  9
569  05  5
570  09  9
571  02  2
572  65  ×
573  43  RCL
574  25   25
575  75  -
576  00  0
577  93  .
578  02  2
579  08  8
580  04  4
581  04  4
582  09  9
583  06  6
584  07  7
585  03  3
586  06  6
587  65  ×
588  43  RCL
589  25   25
590  33  X²
591  85  +
592  01  1
593  93  .
594  04  4
595  02  2
596  01  1
597  04  4
598  01  1
599  03  3
600  07  7
```

PROGRAM FOR PREDICTION OF CASE DEPTH
(One-Dimensional)

601	04	4
602	01	1
603	65	×
604	43	RCL
605	25	25
606	45	Y^x
607	03	3
608	75	-
609	01	1
610	93	.
611	04	4
612	05	5
613	03	3
614	01	1
615	05	5
616	02	2
617	00	0
618	02	2
619	07	7
620	65	×
621	43	RCL
622	25	25
623	45	Y^x
624	04	4
625	85	+
626	01	1
627	93	.
628	00	0
629	06	6
630	01	1
631	04	4
632	00	0
633	05	5
634	04	4
635	02	2
636	09	9
637	65	×
638	43	RCL
639	25	25
640	45	Y^x
641	05	5
642	54	)
643	65	×
644	01	1
645	22	INV
646	23	LNX
647	45	Y^x
648	43	RCL
649	24	24
650	33	X^2
651	94	+/-
652	95	=
653	42	STD
654	26	26
655	01	1
656	22	INV
657	23	LNX
658	45	Y^x
659	43	RCL
660	24	24
661	33	X^2
662	94	+/-
663	55	÷
664	89	π
665	34	$\sqrt{X}$
666	75	-
667	43	RCL
668	24	24
669	65	×
670	43	RCL
671	26	26
672	85	+
673	00	0
674	95	=
675	54	)
676	92	RTN

APPENDIX II

The program listed on the following pages utilizes a one-dimensional heat flow model for the high speed range, and a three-dimensional model for the low speed ranges.

The program is written for use on a Texas Instrument TI 59. programmable calculator with a PC-100 printer.

User Instructions

1. Partition the calculator to mode 799:19 by entering 2 and push 2th op. 17.
2. Enter laser power (watts) in A.
3. Enter speed (cm/sec) in B.
4. Enter thermal conductivity (w/cmC°) in C.
5. Enter thermal diffusivity (cm^2/sec) in D.
6. Enter transformation temperature (C°) in E.
7. Enter size of laser spot (cm) in A^1.
8. Enter room temperature (c°) in B^1.
9. Press C^1. The value of the parameter $B = \nu b/2\alpha$ will be displayed. Now press R/S. The calculator will print surface temperature, depth of case (in cm and mils), the value of the parameter B and the ratio of the parameters Z and B ($Z = \nu z/2\alpha$). The results are valid if:

$$B \gtrsim 0.5$$

$$Z/B \lesssim 0.5 \text{ for } 1 \gtrsim B \gtrsim 0.5$$

$$Z/B \lesssim 0.4 \text{ for } 4 \gtrsim B \gtrsim 1$$

$$\text{for all values of } B \gtrsim 4$$

PROGRAM FOR PREDICTION OF CASE
(Three-Dimensional)

```
000  76  LBL
001  11   A
002  53   (
003  42  STO
004  00   00
005  54   )
006  92  RTN
007  76  LBL
008  12   B
009  53   (
010  42  STO
011  01   01
012  54   )
013  92  RTN
014  76  LBL
015  13   C
016  53   (
017  42  STO
018  02   02
019  54   )
020  92  RTN
021  76  LBL
022  14   D
023  53   (
024  42  STO
025  03   03
026  54   )
027  92  RTN
028  76  LBL
029  15   E
030  53   (
031  42  STO
032  04   04
033  54   )
034  92  RTN
035  76  LBL
036  16  A'
037  53   (
038  42  STO
039  05   05
040  54   )
041  92  RTN
042  76  LBL
043  17  B'
044  53   (
045  42  STO
046  06   06
047  54   )
048  92  RTN
049  76  LBL
050  18  C'
051  53   (
052  43  RCL
053  00   00
054  55   ÷
055  43  RCL
056  05   05
057  33  X²
058  65   x
059  00   0
060  93   .
061  08   8
062  05   5
063  95   =
064  42  STO
065  07   07
066  43  RCL
067  05   05
068  55   ÷
069  43  RCL
070  01   01
071  95   =
072  42  STO
073  08   08
074  43  RCL
075  05   05
076  65   x
077  43  RCL
078  01   01
079  55   ÷
080  04   4
081  55   ÷
082  43  RCL
083  03   03
084  95   =
085  42  STO
086  09   09
087  91  R/S
088  43  RCL
089  04   04
090  75   -
091  43  RCL
092  06   06
093  95   =
094  42  STO
095  10   10
096  02   2
097  00   0
098  35  1/X
099  42  STO
100  11   11
101  01   1
102  42  STO
103  12   12
104  00   0
105  42  STO
106  13   13
107  43  RCL
108  13   13
109  19  D'
110  42  STO
111  14   14
112  85   +
113  43  RCL
114  06   06
115  95   =
116  59  INT
117  99  PRT
118  43  RCL
119  14   14
120  75   -
121  43  RCL
122  10   10
123  95   =
124  32  X:T
125  01   1
126  77   GE
127  01   01
128  90   90
129  43  RCL
130  11   11
131  55   ÷
132  43  RCL
133  12   12
134  95   =
135  42  STO
136  11   11
137  43  RCL
138  13   13
139  85   +
140  43  RCL
141  11   11
142  95   =
143  42  STO
144  13   13
145  43  RCL
146  13   13
147  19  D'
148  42  STO
149  14   14
150  75
```

PROGRAM FOR PREDICTION OF CASE
(Three-Dimensional)

```
151  43  RCL
152  10   10
153  95   =
154  50  I×I
155  32  X:T
156  01   1
157  77   GE
158  01   01
159  90   90
160  43  RCL
161  10   10
162  32  X:T
163  43  RCL
164  14   14
165  77   GE
166  01   01
167  29   29
168  02   2
169  42  STO
170  12   12
171  43  RCL
172  11   11
173  55   ÷
174  43  RCL
175  12   12
176  95   =
177  42  STO
178  11   11
179  43  RCL
180  13   13
181  75   -
182  43  RCL
183  11   11
184  95   =
185  42  STO
186  13   13
187  61  GTO
188  01   01
189  45   45
190  58  FIX
191  04   04
192  43  RCL
193  13   13
194  99  PRT
195  55   ÷
196  02   2
197  93   .
198  05   5
199  04   4
200  65   ×
201  01   1
202  00   0
203  00   0
204  00   0
205  95   =
206  99  PRT
207  98  ADV
208  22  INV
209  58  FIX
210  43  RCL
211  09   09
212  99  PRT
213  43  RCL
214  16   16
215  99  PRT
216  98  ADV
217  54   )
218  92  RTN
219  76  LBL
220  19   D'
221  53   (
222  42  STO
223  13   13
224  55   ÷
225  02   2
226  55   ÷
227  53   (
228  43  RCL
229  03   03
230  65   ×
231  43  RCL
232  08   08
233  54   )
234  34   ΓX
235  95   =
236  10   E'
237  65   ×
238  02   2
239  65   ×
240  43  RCL
241  07   07
242  55   ÷
243  43  RCL
244  02   02
245  65   ×
246  53   (
247  43  RCL
248  03   03
249  65   ×
250  43  RCL
251  08   08
252  54   )
253  34   ΓX
254  95   =
255  42  STO
256  15   15
257  02   2
258  65   ×
259  43  RCL
260  13   13
261  55   ÷
262  43  RCL
263  05   05
264  95   =
265  42  STO
266  16   16
267  01   1
268  42  STO
269  17   17
270  04   4
271  32  X:T
272  43  RCL
273  09   09
274  77   GE
275  06   06
276  37   37
277  02   2
278  32  X:T
279  43  RCL
280  09   09
281  77   GE
282  05   05
283  33   33
284  01   1
285  32  X:T
286  43  RCL
287  09   09
288  77   GE
289  04   04
290  11   11
291  53   (
292  00   0
293  93   .
294  00   0
295  01   1
296  02   2
297  01   1
298  04   4
299  06   6
300  65   ×
```

PROGRAM FOR PREDICTION OF CASE
(Three-Dimensional)

301	43	RCL
302	09	09
303	33	X²
304	85	+
305	00	0
306	93	.
307	00	0
308	05	5
309	06	6
310	00	0
311	06	6
312	05	5
313	65	×
314	43	RCL
315	09	09
316	85	+
317	00	0
318	93	.
319	00	0
320	06	6
321	06	6
322	06	6
323	01	1
324	54	)
325	65	×
326	43	RCL
327	16	16
328	33	X²
329	85	+
330	53	(
331	00	0
332	93	.
333	00	0
334	02	2
335	01	1
336	08	8
337	01	1
338	04	4
339	65	×
340	43	RCL
341	09	09
342	33	X²
343	75	-
344	00	0
345	93	.
346	00	0
347	01	1
348	04	4
349	04	4
350	03	3
351	05	5
352	65	×
353	43	RCL
354	09	09
355	75	-
356	00	0
357	93	.
358	02	2
359	08	8
360	03	3
361	01	1
362	06	6
363	01	1
364	54	)
365	65	×
366	43	RCL
367	16	16
368	85	+
369	53	(
370	00	0
371	93	.
372	00	0
373	06	6
374	05	5
375	05	5
376	01	1
377	65	×
378	43	RCL
379	09	09
380	35	1/X
381	33	X²
382	75	-
383	00	0
384	93	.
385	03	3
386	02	2
387	08	8
388	07	7
389	07	7
390	04	4.
391	65	×
392	43	RCL
393	09	09
394	35	1/X
395	85	+
396	00	0
397	93	.
398	09	9
399	07	7
400	00	0
401	02	2
402	04	4
403	07	7
404	54	)
405	95	=
406	42	STO
407	17	17
408	61	GTO
409	06	06
410	37	37
411	53	(
412	00	0
413	93	.
414	00	0
415	04	4
416	08	8
417	09	9
418	02	2
419	06	6
420	65	×
421	43	RCL
422	09	09
423	33	X²
424	75	-
425	00	0
426	93	.
427	00	0
428	03	3
429	05	5
430	08	8
431	08	8
432	05	5
433	65	×
434	43	RCL
435	09	09
436	85	+
437	00	0
438	93	.
439	01	1
440	02	2
441	01	1
442	07	7
443	08	8
444	54	)
445	65	×
446	43	RCL
447	16	16
448	33	X²
449	75	
450	53	

PROGRAM FOR PREDICTION OF CASE

(Three-Dimensional)

451	00	0
452	93	.
453	00	0
454	01	1
455	02	2
456	09	9
457	02	2
458	02	2
459	65	×
460	43	RCL
461	09	09
462	33	X²
463	75	-
464	00	0
465	93	.
466	00	0
467	07	7
468	02	2
469	04	4
470	00	0
471	05	5
472	65	×
473	43	RCL
474	09	09
475	85	+
476	00	0
477	93	.
478	03	3
479	03	3
480	05	5
481	02	2
482	06	6
483	05	5
484	54	)
485	65	×
486	43	RCL
487	16	16
488	85	+
489	53	(
490	00	0
491	93	.
492	01	1
493	03	3
494	04	4
495	08	8
496	03	3
497	02	2
498	65	×
499	43	RCL
500	09	09
501	35	1/X
502	33	X²
503	75	-
504	00	0
505	93	.
506	04	4
507	04	4
508	04	4
509	02	2
510	09	9
511	06	6
512	65	×
513	43	RCL
514	09	09
515	35	1/X
516	85	+
517	01	1
518	93	.
519	00	0
520	01	1
521	06	6
522	04	4
523	06	6
524	08	8
525	54	)
526	95	=
527	42	STO
528	17	17
529	61	GTO
530	06	06
531	37	37
532	53	(
533	00	0
534	93	.
535	00	0
536	01	1
537	09	9
538	09	9
539	01	1
540	65	×
541	43	RCL
542	09	09
543	33	X²
544	85	+
545	00	0
546	93	.
547	00	0
548	06	6
549	03	3
550	01	1
551	08	8
552	65	×
553	43	RCL
554	09	09
555	85	+
556	00	0
557	93	.
558	00	0
559	01	1
560	01	1
561	54	)
562	65	×
563	43	RCL
564	16	16
565	33	X²
566	75	-
567	53	(
568	00	0
569	93	.
570	00	0
571	00	0
572	05	5
573	08	8
574	06	6
575	65	×
576	43	RCL
577	09	09
578	33	X²
579	75	-
580	00	0
581	93	.
582	00	0
583	04	4
584	08	8
585	04	4
586	65	×
587	43	RCL
588	09	09
589	85	+
590	00	0
591	93	.
592	03	3
593	00	0
594	04	4
595	07	7
596	54	)
597	65	×
598	43	RCL
599	16	16
600	85	+

PROGRAM FOR PREDICTION OF CASE
(Three-Dimensional)

601	53	(	651	00	0	701	02	2
602	00	0	652	93	.	702	01	1
603	93	.	653	03	3	703	04	4
604	01	1	654	02	2	704	01	1
605	01	1	655	07	7	705	03	3
606	02	2	656	05	5	706	07	7
607	03	3	657	09	9	707	04	4
608	03	3	658	01	1	708	01	1
609	65	×	659	01	1	709	65	×
610	43	RCL	660	85	+	710	43	RCL
611	09	09	661	01	1	711	19	19
612	35	1/X	662	95	=	712	45	Y^x
613	33	X^2	663	35	1/X	713	03	3
614	75	-	664	42	STO	714	75	-
615	00	0	665	19	19	715	01	1
616	93	.	666	53	(	716	93	.
617	04	4	667	00	0	717	04	4
618	04	4	668	93	.	718	05	5
619	04	4	669	02	2	719	03	3
620	01	1	670	05	5	720	01	1
621	65	×	671	04	4	721	05	5
622	43	RCL	672	08	8	722	02	2
623	09	09	673	02	2	723	00	0
624	35	1/X	674	09	9	724	02	2
625	85	+	675	05	5	725	07	7
626	01	1	676	09	9	726	65	×
627	93	.	677	02	2	727	43	RCL
628	00	0	678	65	×	728	19	19
629	02	2	679	43	RCL	729	45	Y^x
630	01	1	680	19	19	730	04	4
631	06	6	681	75	-	731	85	+
632	03	3	682	00	0	732	01	1
633	54	)	683	93	.	733	93	.
634	95	=	684	02	2	734	00	0
635	42	STO	685	08	8	735	06	6
636	17	17	686	04	4	736	01	1
637	43	RCL	687	04	4	737	04	4
638	15	15	688	09	9	738	00	0
639	65	×	689	06	6	739	05	5
640	43	RCL	690	07	7	740	04	4
641	17	17	691	03	3	741	02	2
642	95	=	692	06	6	742	09	9
643	54	)	693	65	×	743	65	×
644	92	RTN	694	43	RCL	744	43	RCL
645	76	LBL	695	19	19	745	19	19
646	10	E'	696	33	X^2	746	45	Y^x
647	53	(	697	85	+	747	05	5
648	42	STO	698	01	1	748	54	)
649	18	18	699	93	.	749	65	[illegible]
650	65	×	700	04	4	750	01	1

PROGRAM FOR PREDICTION OF CASE

(Three-Dimensional)

```
751  22 INV
752  23 LNX
753  45 YX
754  43 RCL
755  18  18
756  33 X²
757  94 +/-
758  95  =
759  42 STO
760  19  19
761  01  1
762  22 INV
763  23 LNX
764  45 YX
765  43 RCL
766  18  18
767  33 X²
768  94 +/-
769  55  ÷
770  89  π
771  34 √X
772  75  -
773  43 RCL
774  18  18
775  65  ×
776  43 RCL
777  19  19
778  95  =
779  54  )
780  92 RTN
```

END
FILMED
4-86
DTIC